



Correcting for the clumping effect in leaf area index calculations using one-dimensional fractal dimension

Yongkang Lai^a, Xihan Mu^{a,*}, Weihua Li^a, Jie Zou^b, Yuequn Bian^a, Kun Zhou^a, Ronghai Hu^c, Linyuan Li^d, Donghui Xie^a, Guangjian Yan^a

^a State Key Laboratory of Remote Sensing Science, Institute of Remote Sensing Science and Engineering, Faculty of Geographical Science, Beijing Normal University, Beijing 100875, China

^b The Academy of Digital China (Fujian), Fuzhou University, Fuzhou 350116, China

^c College of Resources and Environment, University of Chinese Academy of Sciences, Beijing 100049, China

^d Key Laboratory for Silvicultural and Conservation of Ministry of Education, Beijing Forestry University, Beijing 100083, China

ARTICLE INFO

Edited by Jing M. Chen

Keywords:

Leaf area index (LAI)
Clumping effect
Clumping index (CI)
Fractal dimension (FD)

ABSTRACT

The clumping effect is the main issue causing the heterogeneity in vegetation canopies and the underestimation of leaf area index (LAI) obtained using indirect measurement methods. Significant efforts have been exerted to correct for the clumping effect and derive the true LAI. Recent research has shown that the fractal dimension (FD) is directly related to the clumping effect of foliage, yet practical methods are needed to calculate field estimates. Considering that widely used LAI applications such as digital hemispherical photography (DHP), tracing radiation and architecture of canopies (TRAC), and digital cover photography (DCP) estimate LAI with one-dimensional (1D) gap probability and gap size data, we propose a method to correct for the clumping effect using 1D FD. Resulting formulae describing the relationship between LAI, CI, and 1D FD were based on the box-counting method (BCM) and a binomial distribution model. Sixty-four simulated scenes including four Radiation transfer Model Intercomparison (RAMI) actual canopies and field measurements from nine plots (four orchard plots and five coniferous forest plots) were used to validate the novel method. Results showed good agreement with reference LAI values for simulated scenes ($R^2 = 0.96$ and $RMSE = 0.35$). The 1DFD method generated higher LAI estimates compared with the LAI measured using TRAC at the four orchard plots especially at high canopy closure, while its results were more consistent with LAI obtained by litter collection than those of comparable methods at coniferous forest plots (bias from -13.5% to 9.9% for DCP images, from -3.0% to 19.7% for DHP images, and from -3.8% to 17.0% for TRAC transects). Our validation efforts indicate that the method proposed herein corrects for the clumping effect of vegetated canopies more effectively with DCP images, DHP images, and TRAC measurement when compared with traditional indirect optical methods. The 1DFD method is expected to improve indirect measurement accuracy of LAI.

1. Introduction

Leaf area index (LAI), defined as half the total leaf area per unit horizontal ground surface area (Chen and Black, 1992; Gonsamo and Pellikka, 2008; Leblanc et al., 2005), has been widely used in research on climate, ecosystem, and hydrological modelling (Asner et al., 2003; Jonckheere et al., 2004; Stark et al., 2012). Remote sensing is a critical tool for deriving LAI at regional and global scales. However, because of the heterogeneity of vegetation structure, it is challenging to provide accurate estimates of LAI using remote sensing methods (Breda, 2003).

Therefore, obtaining accurate *in situ* LAI measurements of vegetation canopies is crucial for calibrating and validating LAI satellite products (Cohen et al., 2003; Qu et al., 2013).

Ground-based LAI estimation methods are classified into two categories: direct and indirect. Direct methods, measuring the area of leaves and calculating LAI from leaf litter or harvested leaves (Fang et al., 2019), can generate relatively accurate estimates of LAI (Qu et al., 2013), but are not suitable for large plots and cannot estimate LAI at large spatial and temporal scales because they are destructive, labor-intensive, and time-consuming (Daughtry, 1990; Gower et al., 1999).

* Corresponding author.

E-mail address: muxihan@bnu.edu.cn (X. Mu).

<https://doi.org/10.1016/j.rse.2022.113259>

Received 21 June 2022; Received in revised form 24 August 2022; Accepted 3 September 2022

Available online 13 September 2022

0034-4257/© 2022 The Authors. Published by Elsevier Inc. This is an open access article under the CC BY license (<http://creativecommons.org/licenses/by/4.0/>).

Indirect methods, generally based on the Beer-Lambert Law, can rapidly produce estimates of LAI and have been widely used in the validation of LAI products (Yan et al., 2019). Theoretically, there should be a very large (virtually infinite) number of leaves in the study area to satisfy the Poisson model assumed underlying the Beer-Lambert Law. However, when the study area is >10 times the leaf area (meaning that there is a sufficient number of leaves), the gap probability obtained from the binominal distribution model differs very little from that obtained by the Poisson model (Lang and Xiang, 1986). Therefore, Beer-Lambert Law can be used to calculate the LAI of an actual plot with finite number of leaves. Additionally, Beer-Lambert Law is suitable for describing the attenuation of light in uniform canopies where the leaves are randomly distributed. However, leaves are generally clumped in canopies. The difficulty with indirect methods lies primarily in how to correct for the clumping effect at different scales (e.g., within-crown and between-crown) (Yan et al., 2019). The clumping index (CI), which describes the deviation of leaf distribution from a random distribution, was proposed to quantify the clumping effect (Black et al., 1991; Nilson, 1971). In the past, considerable efforts were exerted to correct for the clumping effect, including development of the finite-length averaging method (LX) (Lang and Xiang, 1986), gap-size distribution method (CC) (Chen and Cihlar, 1995a; Leblanc, 2002), combination of the CC method and the LX method (CLX) (Leblanc et al., 2005), path length distribution method (PATH) (Hu et al., 2014), etc. The LX method assumes that leaves are randomly distributed within a sub-segment of finite length. Applying the Beer-Lambert Law to each sub-segment and then averaging them can address the clumping effect (Lang and Xiang, 1986). Other commonly applied methods introduce gap size information (e.g., CC and CLX methods) or path length distribution (e.g., PATH method) to quantify the clumping effect. Although these methods can reduce the clumping effect, improvements are necessary to provide a more complete correction of the clumping effect. For example, the LX method cannot address the clumping effect within the sub-segments and thus requires calculation of an appropriate sub-segment length (Yan et al., 2019). The CC method corrects for the clumping effect by removing large gaps between crowns (Chen and Cihlar, 1995a; Gonsamo and Pellikka, 2009) and mainly targets the clumping at the between-crowns scale (Hu et al., 2014; Yan et al., 2016). To resolve deficiencies of the LX method, Leblanc et al. (2005) applied the CC method to each LX sub-segment. Yet, validations showed that the deficiencies of the LX method (e.g., effect of sub-segment length on results) were not completely eliminated (Pisek et al., 2011a). The PATH method addresses both within- and between-crown clumping by introducing a path length distribution based on: (1) a three-dimension (3D) shape of the canopy, or (2) a transect extracted from DCP images or measured by TRAC (Hu et al., 2018a; Hu et al., 2018b). However, using these methods to obtain path length distribution has some problems, such as the influence of mutual occlusion between tree crowns on obtaining complete 3D shapes of canopies, which affect the LAI estimate.

To meet the increasing accuracy required by more recent applications, new methods should be developed to comprehensively correct for clumping effects. Fractal dimension (FD) is a measurement of complexity of spatial filling (Alados et al., 1999) and has been applied to quantitatively characterize the spatial dispersion of leaves within the crown (Jonckheere et al., 2006). The FD has been proven to be directly related to foliage clumping (Jonckheere et al., 2006). Generally, a large FD implies low heterogeneity (Alados et al., 1999). Some studies have tried to introduce the FD to the Beer-Lambert Law as a correction factor to increase LAI measurement accuracy (Foroutan-pour et al., 2001; Jonckheere et al., 2006; Nackaerts et al., 1999). Recently, Li and Mu derived a mathematical relationship between LAI, CI, and the two-dimensional (2D) FD calculated from digital cover photography (DCP) images based on the box-counting method (BCM) and a Boolean model (Li and Mu, 2021). The 2DFD method was proven to be applicable to DCP images. However, it cannot be used with one-dimensional (1D) data such as the data obtained by tracing the radiation and architecture of

canopies (TRAC) or transects extracted from digital hemispherical photography (DHP) and DCP imagery.

Since 1D data account for a large proportion of field measurement data, it is worth exploring how to use this 1D information and establish a relationship between 1D FD, LAI, and CI. In this paper, we established a mathematical relationship between 1D FD, CI, and LAI, that can be applied to DCP images, DHP images, and TRAC data. Then, those types of data were used to assess the 1DFD method and other 1D methods (i.e., CC method, CLX method, and PATH method). For comparison with the 2DFD method, the major data source for this study was DCP imagery. Sixty simulated scenes (12 homogeneous canopies, 21 discrete spherical crown vegetation canopies, and 27 realistic forest canopies), four Radiation transfer Model Intercomparison (RAMI) actual canopies, and nine field plots (four orchard plots and five coniferous forest plots) were used to comprehensively assess the 1DFD method and the comparable methods.

2. Mathematical relationship between FD, LAI, and CI

Firstly, the BCM is introduced to calculate the 1D FD of transects. Next, we theoretically deduce the 1D FD of horizontally and randomly distributed leaves and establish the relationship between the 1D FD and LAI. Then, the influence of leaf angle and leaf clumping on the relationship between 1D FD and LAI is considered. Finally, the implementation of the 1DFD method and the comparison methods are illustrated. Before describing the details of the method derivation, some notations and definitions are presented in Table 1 for convenience.

2.1. Calculating 1D FD based on BCM

The BCM is the method most frequently used to calculate the 2D FD, because of its practicality and simplicity (Foroutan-pour et al., 1999a; Li et al., 2009). In this method, non-overlapping boxes cover the entire image and are divided into two categories: boxes containing pixels with target objects (e.g., leaves), and boxes containing pixels not covering target objects (Fig. 1). A series of the number of boxes containing target objects, recorded as $N(a)$, are obtained by changing box size (a). The FD, then, is the absolute value of the slope of the regression line between the logarithms of $N(a)$ and a (Bisoi and Mishra, 2001; Foroutan-pour et al.,

Table 1

Notations and definitions of variables for method deduction.

Name	Notations and definitions	Name	Notations and definitions
a	Length of the box for calculating the FD of the image in the BCM;	σ	Leaf area of a single leaf;
s	Length of FD segment for calculating the FD of the transect in the BCM;	w	Leaf width;
$N(a)$	Number of boxes containing target objects (e.g., leaf) in the BCM;	P_L	Probability of a leaf in an image intersecting a transect;
$N(s)$	Number of FD segments containing target objects (e.g., leaf) in the BCM;	P_s	Probability of an FD segment intersecting leaf chords on a transect;
A	Surface area represented by an image;	\overline{P}_s	Probability of an FD segment not intersecting with any leaf chord on a transect;
N_L	Number of leaves in an image;	θ	Zenith angle;
N_F	Number of FD segments along a transect of length L ;	$P(\theta)$	Gap probability at zenith θ ;
N_C	Number of leaves intersecting a transect, i.e., the number of leaf chords along a transect;	Ω	Clumping index;
l	Transect length;	Ω_E	Clumping index at scales larger than the shoots;
l_c	Average length of all chords of a leaf;	α	Woody-to-total area ratio;
		γ_E	Needle-to-shoot area ratio;

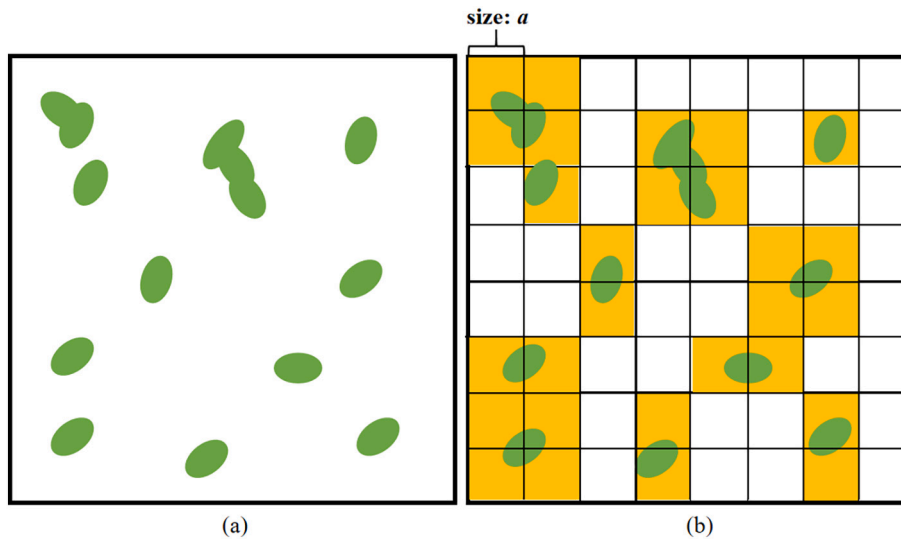


Fig. 1. These two images represent the calculation of fractal dimension using BCM. (a) An illustration with leaves and (b) the same illustration covered by non-overlapping boxes (yellow and white grid cells) of size a . Yellow boxes contain leaf pixels. White boxes do not. (For interpretation of the references to colour in this figure legend, the reader is referred to the web version of this article.)

1999a, 1999b).

$$\ln(N(a)) = -FD \cdot \ln(a) + b \tag{1}$$

where b is the intercept for the regression line.

The calculation of 1D FD mimics the BCM process, where the target objects in the 1D space are no longer leaves on a 2D digital image but are instead leaf chords on a 1D transect (Fig. 2). The boxes in the BCM become 1D segments (Fig. 2; called FD segments hereafter). The FD formula remains unchanged (Eq. (1)), although a and $N(a)$ now represent the size and the number of 1D FD segments that intersect with a leaf chord, respectively. For ease of distinction, the a and $N(a)$ of 1D FD will be expressed as s and $N(s)$ hereafter.

The FD is invariant within a certain scale (Alados et al., 1999; Berntson and Stoll, 1997). Specifically, the FD of a self-similar geometric structure could keep the same in all length scales, while the FD of natural objects is statistically invariant over limited range of scales. Therefore, we should determine a specific value or a range of s where the FD is calculated as the derivative of $\ln(N(s))$. When BCM is used to calculate the FD of an image, the size of the box is confined to a certain range of spatial scales (Berntson and Stoll, 1997; Foroutan-pour et al., 1999a).

Similarly, the selection of a proper s is necessary for obtaining a reasonable FD to reflect the distribution of leaves along a transect. The FD will merely represent the clumping of crowns if the s is too long (e.g., the size of the tree crown), and will be greatly affected by the leaf shape if the s is too short (e.g., the leaf size). Thus, s was set to ten times the leaf radius ($s = 10r$) in this study. The impact of the FD segment length for the 1DFD method is discussed in Section 4.4.1.

Next, we deduce the quantitative relationship between 1D FD, LAI, and CI based on the principle of BCM.

2.2. The 1D FD of horizontally and randomly distributed leaves

First, we need to establish a relationship between $N(s)$ in 1D FD and the LAI for a simple case in which leaves are horizontally and randomly distributed. The number of FD segments (N_F), along a transect of length l , is given as $N_F = \frac{l}{s}$. If the probability of an FD segment intersecting leaf chords is P_s , $N(s)$ is the expectation of a binomial distribution model under the assumption of random and horizontal distribution of leaves, and is expressed as $N(s) = N_F P_s$. The P_s can be calculated together with the probability that an FD segment does not intersect with any leaf chord

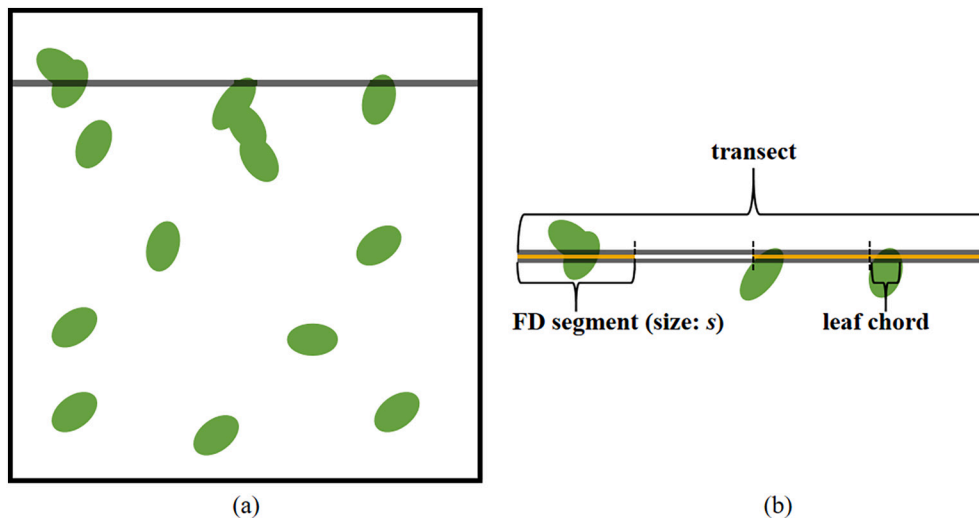


Fig. 2. An example of a 1D transect that illustrates the 1D FD where (a) is a picture with leaves and a transect (translucent black line) and (b) is the transect extracted from (a) and covered by FD segments (yellow and white line segments) of size s . The three yellow FD segments in (b) are those that intersect with leaf chords, while the one white FD segment indicates it does not intersect with any leaf chords. (For interpretation of the references to colour in this figure legend, the reader is referred to the web version of this article.)

on a transect, i.e., $\overline{P_s}$, as follows:

$$P_s = 1 - \overline{P_s} = 1 - \left(1 - \frac{s + l_c}{l}\right)^{N_C} \quad (2)$$

where l_c is the average length of all chords of a leaf, and $\frac{s+l_c}{l}$ is the probability that an FD segment intersects with a randomly distributed leaf chord along the transect (Fig. 3), while N_C is the number of leaf chords on a transect. The N_C can be expressed as:

$$N_C = N_L \frac{l_w + \sigma}{A} \quad (3)$$

where σ is the leaf area of a single leaf, w is the leaf width, A is surface area represented by an image, and N_L is the number of leaves in an image. The specific derivation processes of N_C and l_c are described in Appendices A and B, respectively.

The leaf shape is assumed to be circular in this study. Thus, σ equals πr^2 and w equals $2r$, where r is the leaf radius, expressed by the unit of pixels. The l_c is related to leaf shape. For a circular leaf, $l_c = \frac{\pi r}{2}$ (Appendix B).

Combining $N(s) = N_r P_s$ and Eqs. (2) and (3), and $l_c = \frac{\pi r}{2}$, we can estimate $N(s)$ as:

$$N(s) = \frac{l}{s} (1 - Q^T) \quad (4)$$

where $T = \frac{2rN_L l + N_L \pi r^2}{A}$ and $Q = 1 - \frac{\pi r + 2s}{2l}$.

Taking the first derivative of Eq. (1), the FD can then be expressed as:

$$FD = \left| \frac{d \ln(N(s))}{d \ln(s)} \right| \quad (5)$$

From Eqs. (4) and (5), we can drive the FD of randomly and horizontally distributed leaves:

$$FD_d = 1 - \frac{s \cdot T Q^{T-1}}{l \cdot (1 - Q^T)} \quad (6)$$

Considering the derivative of Eq. (1) with the s equal to $10r$ (Section 2.1) and $LAI = \frac{N_L \pi r^2}{A}$, a relationship between FD and LAI can be obtained from Eq. (6) as follows:

$$FD_d = 1 - \frac{10LAI(2l + \pi r) \cdot H_d}{\pi l(1 - H_d \cdot V_d)} \quad (7)$$

where

$$H_d = \exp\left(-LAI - \frac{20LAI}{\pi}\right) \cdot V_d^{LAI-1} \quad (8)$$

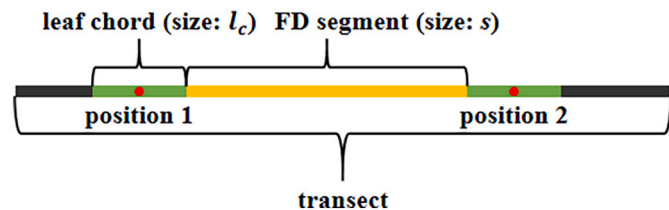


Fig. 3. The probability that an FD segment intersects with a randomly distributed leaf chord on a transect is shown. An FD segment (yellow segment) of length s is fixed on a transect (the entire line) of length l . To ensure that the leaf chord (green segments) of length l_c intersects with the FD segment, the center of the leaf chord (red points) can only be located within the range from position 1 to position 2. Positions 1 and 2 are where the leaf chord and FD segment begin to intersect. The moving length of the center of the leaf chord is $s + l_c$, and the total length of the transect is l , so the probability for intersection is $\frac{s+l_c}{l}$. (For interpretation of the references to colour in this figure legend, the reader is referred to the web version of this article.)

and

$$V_d = 1 - \frac{\pi r + 20r}{2l} \quad (9)$$

The process of deriving Eqs. (7)–(9) from Eq. (6) is described in detail in the Appendix C.

2.3. The consideration of leaf angle and CI

The effect of leaf angle distribution (LAD) has been widely recognized and can be described by the leaf projection function $G(\theta)$ in which θ refers to the zenith angle (Ross, 1981; Wang et al., 2007; Wilson, 1960). According to the definition of $G(\theta)$, the average area of a single leaf projected on the plane perpendicular to the view direction is defined as $G(\theta)\pi r^2$. The change of leaf area σ into the mean projected leaf area influences the relationship between FD and LAI. The N_C is changed to:

$$N_C = N_L \frac{2\sqrt{G(\theta)}lr + G(\theta)\pi r^2}{A} \quad (10)$$

The l_c becomes:

$$l_c = \frac{\pi r \sqrt{G(\theta)}}{2} \quad (11)$$

Generally, leaves are not randomly distributed; they are clumped. Indirect estimates of LAI are underestimated due to this clumping effect, and this underestimation can be between 30% and 70% for forests (Chen and Cihlar, 1995b; Stenberg, 1996), and approximately 11% for row crops (Baret et al., 2010). A parameter commonly represented by Ω in the formula and called the clumping index (CI) was introduced by Nilson (1971) to quantify the clumping effect. The Ω is defined as the ratio of effective LAI (LAI_e) and LAI (Black et al., 1991; Chen and Black, 1991):

$$\Omega = \frac{LAI_e}{LAI} \quad (12)$$

We retain the same form of the second power of Ω when considering the clumping effect for FD as that of Li and Mu (2021), i.e., the LAI in Eqs. (7) and (8) is replaced by $LAI_e \cdot \Omega$. Thus, when considering the influence of leaf angle (Eqs. (10) and (11)) and leaf clumping on Eqs. (7)–(9), the mathematical relationship between LAI_e , FD, and CI (called 1DFD method hereafter) becomes:

$$FD_c = 1 - \frac{10LAI_e \cdot \Omega(2l \cdot \sqrt{G(\theta)} + \pi r \cdot G(\theta)) \cdot H_c}{\pi l(1 - H_c \cdot V_c)} \quad (13)$$

where

$$H_c = \exp\left(-\left(G(\theta)LAI_e \cdot \Omega + \frac{20LAI_e \cdot \Omega \sqrt{G(\theta)}}{\pi}\right)\right) \cdot V_c^{G(\theta)LAI_e \cdot \Omega - 1} \quad (14)$$

and

$$V_c = 1 - \left(\frac{\pi \sqrt{G(\theta)}}{2} + 10\right) \frac{r}{l} \quad (15)$$

The Eq. (13) shows that the relationship between 1D FD and CI is not fixed but affected by other parameters, e.g., LAI and $G(\theta)$.

2.4. Correcting for clumping effect using the 1DFD method

The 1DFD method corrects for clumping effect based on the FD information of transect data. It can be used for DCP images, DHP images, and TRAC transect data to estimate LAI. Since DCP images and DHP images are 2D data, transects need to be extracted from them. To maintain the spatial distribution information of leaf chords, each row of a DCP image is treated as a transect for the 1DFD method. The rings with

zenith being $55^\circ - 60^\circ$ of a DHP image are treated as transects and are used to estimate LAI (Calders et al., 2018b; Jupp et al., 2009), because $G(\theta)$ in this particular direction is almost independent of leaf angle distribution and equals to 0.5 (Ross, 1981; Wilson, 1963).

We must determine $G(\theta)$, the gap probability $P(\theta)$ at zenith θ , r , and 1D FD before implementing the method on transect data. The $G(\theta)$ can be either measured during a field campaign or assumed to be equal to 0.5 (Chianucci and Cutini, 2013; Goudriaan, 1988). The $P(\theta)$ can be obtained by classifying the pixels of a transect into vegetation and non-vegetation (i.e., the proportion of the non-vegetated pixels in the transect). The r can be estimated from the projected area of the leaf. Then, LAI_e can be obtained using Eq. (16) (Ryu et al., 2010) with $G(\theta)$ and $P(\theta)$:

$$LAI_e = \frac{-\ln(P(\theta)) \cdot \cos(\theta)}{G(\theta)} \quad (16)$$

Therefore, the unknown in Eq. (13) is Ω , which can be determined with the 1D FD and Eq. (13). The 1D FD is calculated as the local derivative value of Eq. (1) using BCM in which the FD segment sizes are set to $10r$ and $10r \pm r$ to fit the linear relationship between $\ln(N(s))$ and $\ln(s)$.

The LAI for a transect is calculated using Eq. (12) with the Ω and LAI_e . The LAI for a plot is calculated as the average of LAI of all the transects from DCP images, DHP images, or TRAC measurements in this study.

When considering the effect of woody component on the measured $P(\theta)$, the LAI estimate of the 1DFD method should be regarded as a plant area index (PAI), which is the sum of the LAI and the woody area index (WAI) (Neumann et al., 1989). The woody-to-total area ratio (α) is used in the 1DFD method to convert PAI to LAI as follows (Chen et al., 1997; Zou et al., 2009):

$$LAI = (1 - \alpha) \cdot PAI \quad (17)$$

The Ω in Eq. (13) can only represent the clumping at scales larger than the foliage, which is the overall clumping for broad-leaved species. For coniferous species, shoots are identified as foliage (Chen and Cihlar, 1995a), and the overall clumping is affected by clumping at scales larger than the shoots (Ω_E) plus clumping within the shoots (Chen and Cihlar, 1995a; Fang, 2021; Stenberg et al., 2014). Therefore, the Ω in Eq. (13) is essentially Ω_E for the coniferous forest. To obtain an overall Ω , a needle-to-shoot area ratio (γ_E) is introduced in the 1DFD method to account for within-shoot clumping (Eq. (18)). For broad-leaved species, γ_E is equal to 1.

$$\Omega = \frac{\Omega_E}{\gamma_E} \quad (18)$$

2.5. Comparison of CC, CLX, PATH, and 2DFD methods

We compared our results with the CC, CLX, PATH, and 2DFD methods for cross-validation. Similar to the 1DFD method, these four methods cannot correct for the clumping within shoots and the woody component effect. Therefore, when applying these four methods and the 1DFD method to coniferous forests, γ_E and α are needed to consider the clumping within shoots and eliminate the woody component effect to obtain LAI. When applying these methods to broad-leaved forests, only α is needed to eliminate the woody component effect.

Three metrics including root mean square error (RMSE), coefficient of determination (R^2) and relative difference (RD) were used for quantitative evaluation. RMSE and R^2 respectively assess the difference and the linear relationship between the reference LAI and the calculated LAI. RD is ratio of the difference between the calculated LAI and the reference LAI to the reference LAI (Eq. (19)).

$$RD = \frac{LAI_{cal} - LAI_{ref}}{LAI_{ref}} \times 100\% \quad (19)$$

where LAI_{cal} is the LAI_e or calculated LAI using the CC, CLX, PATH,

2DFD, or 1DFD methods, and LAI_{ref} is the reference LAI.

3. Materials

3.1. Simulation data

The large-scale emulation system (LESS) (Qi et al., 2019) was chosen to simulate three types of scenes, including homogeneous canopies, discrete spherical crown vegetation canopies, and realistic forest canopies (Fig. 4). The 3D object creation tool in LESS can build a vegetation crown without branches by employing structural parameters such as crown shape, crown size, LAD, the number of leaves in a crown, leaf shape, and leaf area. These crowns can be used to create complex canopy scenes by controlling environmental variables, such as distribution of crowns and scene size. The solar and view angles were fixed at zenith to avoid the emergence of shadows that affect classification accuracy for vegetated pixels. The reflectance and transmittance of leaves remained the default values of 0.058 and 0.056, respectively, and the default value of soil reflectance was 0.19. Leaf shapes include circular and non-circular shapes. Non-circular leaf scenes were used to validate the effect of leaf shape on results from the 1DFD method. With the exception of the realistic forest canopy scenes with non-circular leaves, the LAD was spherical. To avoid the effect of woody components, simulated scenes did not contain branches. A downward-facing ortho DCP image with 1.0 cm resolution was generated for each scene to provide gap information for the five comparable methods. The ortho images of the whole scene facilitate the comparison of indirect methods by excluding the factors of camera and manipulator.

Twelve homogeneous scenes were simulated, in which the leaves were randomly distributed. The $G(\theta)$ was 0.5 since the LAD was spherical (Goudriaan, 1988). Leaf area was 0.0079 m^2 , and the radius of the leaf was 0.05 m. The LAI varied from 0.39 to 4.65 for circular leaf scenes and from 0.50 to 2.49 for square leaf scenes (Table 2). The $P(0)$ varied from 0.10 to 0.82 for these homogeneous scenes. Since the estimate accuracy of the LAI was greatly affected by the calculation accuracy of the $P(0)$, when the $P(0)$ was small, homogeneous scenes with a large LAI (e.g., $LAI > 5$) were not simulated.

There were 21 discrete spherical crown vegetation canopy scenes. Each crown was composed of circular or non-circular (square) leaves randomly distributed within the spherical volume. The $G(\theta)$, single leaf area, and radius were the same as for the homogeneous scenes. A Poisson distribution was used for the crowns in these scenes. The LAI varied from 1.10 to 7.61 for circular leaf scenes and 0.91 to 6.00 for non-circular leaf scenes (Table 3). The $P(0)$ varied from 0.13 to 0.68 for circular leaf scenes and from 0.17 to 0.68 for non-circular leaf scenes, respectively. Scenes of different sizes were simulated to account for tree crowns of different sizes. Canopies with a large crown radius corresponded to a large scene size. The simulation of images with different dimensions ensured that the image resolution was the same (1.0 cm) for all scenes. Scenes ranged from $10 \text{ m} \times 10 \text{ m}$ and $1000 \text{ pixel} \times 1000 \text{ pixel}$ to $50 \text{ m} \times 50 \text{ m}$ and $5000 \text{ pixel} \times 5000 \text{ pixel}$.

Twenty-seven realistic forest canopy scenes (15 with circular leaves and 12 with non-circular leaves) were simulated. For circular leaf scenes, each crown was composed of circular leaves randomly distributed within the conal volume. The LAD, single leaf area, and distribution of the crowns were the same as those for the discrete spherical crown vegetated canopy scenes. Nineteen trees in the Wytham Woods 3D model offered by RAMI (Calders et al., 2018a) were selected to create non-circular leaf scenes. Each tree with non-circular (tetragon) leaves in this model was constructed using highly detailed 3D terrestrial laser scanning (TLS) data (Calders et al., 2018a). For each tree, branch and leaf architecture was stored in separate obj-files. We used only the leaf obj-files. Crown position was manually controlled to ensure that crowns did not overlap. The LAI and $P(0)$ of the 15 circular leaf scenes ranged from 1.01 to 5.86 and from 0.08 to 0.65, respectively. The LAI and $P(0)$ of the 12 tetragon leaf scenes varied from 1.09 to 7.13 and from 0.14 to

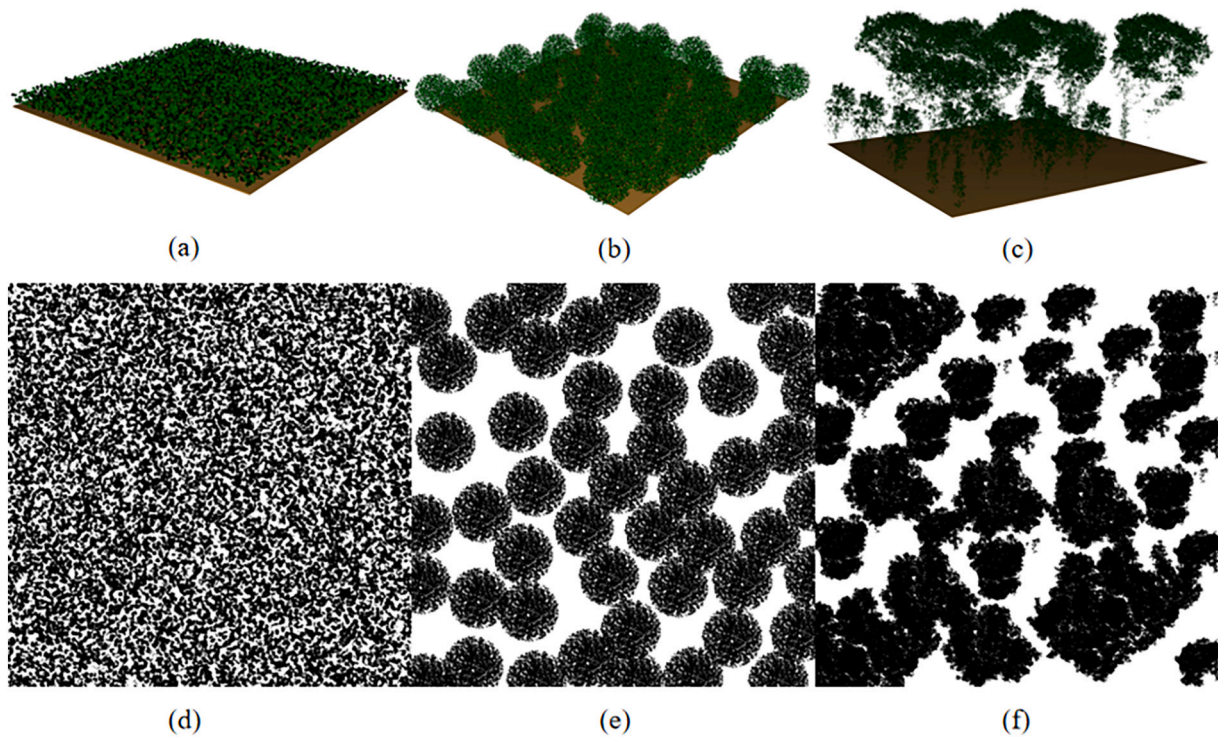


Fig. 4. An example of three types of simulated scenes: (a) homogeneous canopy, (b) discrete spherical crown vegetation canopy, and (c) realistic forest canopy. (d), (e), and (f) represent the ortho DCP images for (a), (b), and (c), respectively.

Table 2
Characteristics of homogeneous scenes.

Leaf shape	Circle	Square
Scene dimension (m × m)	10 × 10	10 × 10
Image dimension (pixel × pixel)	1000 × 1000	1000 × 1000
Total number of scenes	8	4
LAI of scene	0.39, 0.78, 1.09, 1.40, 1.94, 3.10, 3.72, 4.65	0.50, 0.80, 1.50, 2.49
Leaf radius (m)	0.05	
LAD	Spherical distribution	
Leaf width (pixel)	5	

Table 3
Characteristics of discrete spherical crown vegetated canopy scenes.

Leaf shape	Circle	Square
Scene dimension (m × m)	10 × 10, 20 × 20, 50 × 50	10 × 10, 20 × 20
Image dimension (pixel × pixel)	1000 × 1000, 2000 × 2000, 5000 × 5000	1000 × 1000, 2000 × 2000
Crown radius (m)	3, 4, 6	3, 4
Total number of scenes	12	9
LAI of scene	1.10, 1.27, 1.33, 1.54, 1.75, 2.37, 2.62, 2.83, 3.26, 4.19, 6.20, 7.61	0.91, 1.97, 2.28, 2.57, 2.78, 3.29, 4.14, 5.49, 6.00
Leaf radius (m)	0.05	
LAD of scene	Spherical distribution	
Leaf width (pixel)	5	

0.78 (Table 4), respectively. Similar to the discrete spherical crown vegetated canopy scenes, scenes of different sizes were simulated to adapt to tree crowns of different sizes. All ortho DCP images had a resolution of 1.0 cm. When the LAI of circular leaf scenes was equal to 1.68, 2.46, 4.90, and 5.86, however, images with a resolution of 5.0 cm and 0.5 cm were also generated. The 5.0 cm and 0.5 cm resolutions

Table 4
Characteristics of realistic forest canopy scenes.

Leaf shape	Circle	Tetragon
Scene dimension (m × m)	10 × 10, 20 × 20	20 × 20, 50 × 50
Image dimension (pixel × pixel)	400 × 400, 1000 × 1000, 2000 × 2000, 4000 × 4000	2000 × 2000, 5000 × 5000
Total number of scenes	15	12
LAI of scene	1.01, 1.29, 1.68, 1.91, 2.12, 2.46, 2.86, 2.88, 3.52, 3.87, 4.57, 4.67, 4.90, 5.64, 5.86	1.09, 2.09, 2.59, 2.71, 2.98, 3.26, 3.30, 4.13, 4.15, 4.83, 5.52, 7.13

corresponded images with dimensions of 400 × 400 pixels and 4000 × 4000 pixels, respectively. These images with different resolutions were used to assess the impact of image resolution on accuracy.

3.2. RAMI canopy scenes

Four RAMI actual canopies, *i.e.*, Järvelja Pine Stand (Summer), Ofenpass Pine Stand (Winter), Järvelja Birch Stand (Summer), and Wytham Wood were chosen to further compare and validate the methods. The Järvelja Pine Stand (Summer), Ofenpass Pine Stand (Winter), and Järvelja Birch Stand (Summer) were created based on inventory data (Kötz et al., 2004; Kuusk et al., 2009; Kuusk et al., 2013; Kuusk et al., 2010; Kuusk et al., 2008; Morsdorf et al., 2006; Morsdorf et al., 2004). The Järvelja Pine Stand (Summer) and Ofenpass Pine Stand (Winter) were coniferous canopies, while the Järvelja Birch Stand (Summer) and Wytham Wood were broadleaved canopies. For each tree in these four actual scenes, branch and leaf architecture was stored in separate obj-files. Both the branch and leaf architectures were input into LESS to simulate orthographic DCP images with the resolution of 1.0 cm. The location of each tree was provided by RAMI. Consequently, these scenes were more complex and realistic than the scenes mentioned in Section 3.1. Since the tree architecture information was provided by

RAMI, we could calculate the true LAI, $G(\theta)$ at nadir direction ($G(0)$), γ_E , and α (Li and Mu, 2021). The fractional vegetation cover (FVC), LAI, $G(0)$, γ_E , and α are presented in Table 5.

3.3. Field experiments

3.3.1. Orchard plots

We chose nine plots to perform field measurements. Four of them were located in Huailai, Hebei Province, China (Fig. 5 (a)), and the others were located in Chengde, Hebei Province, China (Fig. 5 (b)). The plots in Huailai were apricot orchards with a slope of about 0° , and the trees were planted in rows. Field measurements were conducted in sample plots 1, 2, and 3 on July 30–31, 2019, and in sample plot 4 on May 10, 2021, under clear, windless weather conditions. Considering that orchard pruning and harvest have a great impact on the litter collection method, we used a TRAC instrument to get reference LAI. The TRAC instrument was operated in a solar zenith angle about 45° . According to the instructions, the experimenters walked at a uniform speed in the plots with the TRAC instrument in hand and avoided their shadow blocking the probe. Markers were set every 10 m. The lengths of TRAC transects walked in a cross pattern for plots 1–4 were 95 m, 91 m, 105 m, 134 m, respectively. TRAC recorded the photosynthetic photon flux density (PPFD). According to the total gap probability of the transect provided by TRAC, an appropriate PPFD was selected as a threshold to classify the TRAC data into gaps and canopy elements (i.e., leaves and branches). The classified TRAC data was then processed to calculate PAI for each plot. The woody-to-total area ratio (α) consistent with the default value of 0.05 from the TRAC was used to convert PAI to LAI.

A DJI Mavic Pro unmanned aerial vehicle (UAV; DJI Technology Co., Ltd. Shenzhen, China) was used to take pictures vertically downward at a height of 30 m. The UAV was equipped with a 12-megapixel camera with a wide-angle lens (field of view equals 78.8°). For each plot, six 35-m-long flight routes parallel to the boundaries of the plot were planned, and the distance between two routes was about 6.5 m. Therefore, the actual flying area of the UAV was slightly larger than the plot area. Given the overlap between images, 10 images were selected for each plot. To reduce distortions due to the camera field of view, the UAV image edges were removed. While the original image was 4000 pixel \times 3000 pixel, the cropped image was 1200 pixel \times 800 pixel. The field of view of the cropped image was about 23.4° in the row direction and about 15.7° in the column direction, and the resolution was approximately 1.5 cm. Pixels in the cropped images were classified into leaf and background (soil and branch) pixels using the SHAR-LABFVC method (Song et al., 2015), which has a robust performance on shadow resistance. An image was first transformed into the hue saturation intensity colour space to decrease the difference between sunlit and shaded leaves using intensity histogram equalization. Then, the image was transformed into the LAB colour space, and leaf and background (soil and branch) were distinguished using the green - red component. Based on visual interpretation and validation, the RMSE of the SHAR-LABFVC was 0.025. The LAD was considered spherical, so the $G(\theta)$ equals 0.5 (Goudriaan, 1988). Leaf radius (r) was measured by calculating the projected area of apricot leaves from the UAV images. For each orchard plot, we calculated the LAI of ten cropped UAV images and then averaged the LAI

Table 5

Structural information of four RAMI actual canopies. γ_E and α are the needle-to-shoot area ratio and woody-to-total area ratio, respectively. $G(0)$ is calculated as the ratio of the projected canopy element (i.e., leaf and branch) area at nadir direction to total canopy element area.

Plot	FVC	LAI	α	γ_E	$G(0)$
Järvselja Pine Stand (Summer)	0.41	2.30	0.45	1.48	0.44
Ofenpass Pine Stand (Winter)	0.12	0.74	0.33	0.87	0.39
Järvselja Birch Stand (Summer)	0.50	3.44	0.30	1	0.48
Wytham Wood	0.91	5.16	0.21	1	0.70

of all ten images to derive an LAI for each plot. The average gap probability of ten images was used to calculate an LAI_e for each plot (Ryu et al., 2010).

3.3.2. Conifer forest plots

The remaining five forest plots with a size of 25 m \times 25 m are located in Chengde, Hebei Province, China (Zou et al., 2018). The plots are on flat terrain, and the dominant tree species is *Larix principis-rupprechtii* Mayr. Reference LAI, DCP imagery, DHP imagery, TRAC data, needle-to-shoot area ratio (γ_E), woody-to-total area ratio (α), and other structural parameters were collected during the field campaign (Table 7). The litter collection method, considered the most accurate for estimating LAI in deciduous stands (Chen et al., 1997; Chianucci and Cutini, 2013; Dufrene and Bréda, 1995; Goudriaan, 1988), was used to obtain reference LAI values for the five plots. To ensure that the LAI represented the entire plot, nine traps were placed evenly on a grid at 0.5 m above the ground in each plot, with a distance of 6.25 m between each trap (Zou et al., 2020). The volume of the trap was approximately 0.5 m \times 0.5 m \times 0.5 m. The calculation of reference LAI of each plot was described by Zou et al. (2018).

The upward-facing DCP images were collected on 16 sampling points in each plot which were uniformly distributed within the plot with a 5-m distance. The images were taken with a Canon EOS 6D camera equipped with a Canon 24–70 mm lens between August 11 and September 3, 2017. The camera was mounted on a tripod about 1.2 m from the ground. All images had a dimension of 5472 pixel \times 3648 pixel and were collected under uniform sky conditions. To reduce distortions due to the camera field of view, the centers of images were clipped to 2227 pixel \times 2061 pixel (a field of view of approximately $15^\circ \times 15^\circ$). Meanwhile, DHP images were collected using the same sampling scheme as that of DCP images. The Canon 6D camera equipped with a Sigma 8 mm fisheye lens was used to collect DHP images with a resolution of 5472 pixel \times 3678 pixel before sunrise, after sunset, or under an overcast sky. The procedure described in Gonsamo and Pellikka (2008) was used to preprocess the collected DHP images. Then, the rings with zenith being $55^\circ - 60^\circ$ of the preprocessed DHP images were extracted and used to estimate LAI.

The TRAC measurements were conducted at a height of approximately 1.2 m under clear days. The length of TRAC transects ranged from 100 m to 170 m. The TRAC transects with the zenith angle at approximately 57° were processed as the procedure described in Section 3.3.1, and were then used to estimate LAI. Due to instrument failure, the TRAC measurements were only conducted in plots 5, 7, and 9.

Six to twelve conifer shoots used for the γ_E measurement were picked at each plot. The shoot projection area and half of total needle area of all the picked shoots in the plot were used to calculate the γ_E , after being measured by applying the volume displacement method (Chen et al., 1997). Two to three representative trees near each plot were harvested to measure α . The area of the woody components of harvested trees was calculated by assuming that the trunks and branches at 1.2 m above the ground (equaled to the height of TRAC measurement and photography) were circular truncated cones and the fruits were spheroids. The leaf area of each harvested tree was obtained from the regression relationship between leaf area and leaf dry weight. The leaf area and woody component area were used to calculate α . More details on the field campaign could be found in literature (Zou et al., 2018; Zou et al., 2020).

For each coniferous forest plot, we calculated the PAI for all sixteen DCP images and sixteen DHP images from different sampling points and then obtained the LAI for each image using the γ_E and α (Table 7). We averaged the LAI of sixteen DCP / DHP images to derive an LAI for each plot. The average gap probability of sixteen images was used to calculate an LAI_e for each plot (Ryu et al., 2010). Additionally, the PAI values of TRAC transects of plots 5, 7, and 9 were calculated, and then were converted to LAI with the γ_E and α .



Fig. 5. (a) Apricot orchard located in Huailai, Hebei Province, China. (b) Coniferous forest located in Chengde, Hebei Province, China.

4. Results and discussion

4.1. LAI estimates for simulated scenes

4.1.1. Circular leaf scenes

The $P(0)$, CI, 1D FD, and 2D FD of the 35 simulated circular leaf scenes were calculated. For the sake of brevity, some similar scenes are not shown in Table 8. The 1D FD and 2D FD of homogenous scenes are

approximately 1 and 2, respectively, except for two homogenous scenes where the LAI is <1. In contrast, the 1D FD and 2D FD of the heterogenous scenes are <1 and 2, respectively.

The LAI_e and LAI values derived from the DCP images of these simulated scenes using the CC (LAI_{CC}), CLX (LAI_{CLX}), PATH (LAI_{PATH}), 2DFD (LAI_{2DFD}), and 1DFD (LAI_{1DFD}) methods are presented in Fig. 6. The LAI_e calculated using Eq. (16) was consistent with the true LAI (LAI_{ref}) of the homogenous scenes, while the LAI_e underestimated

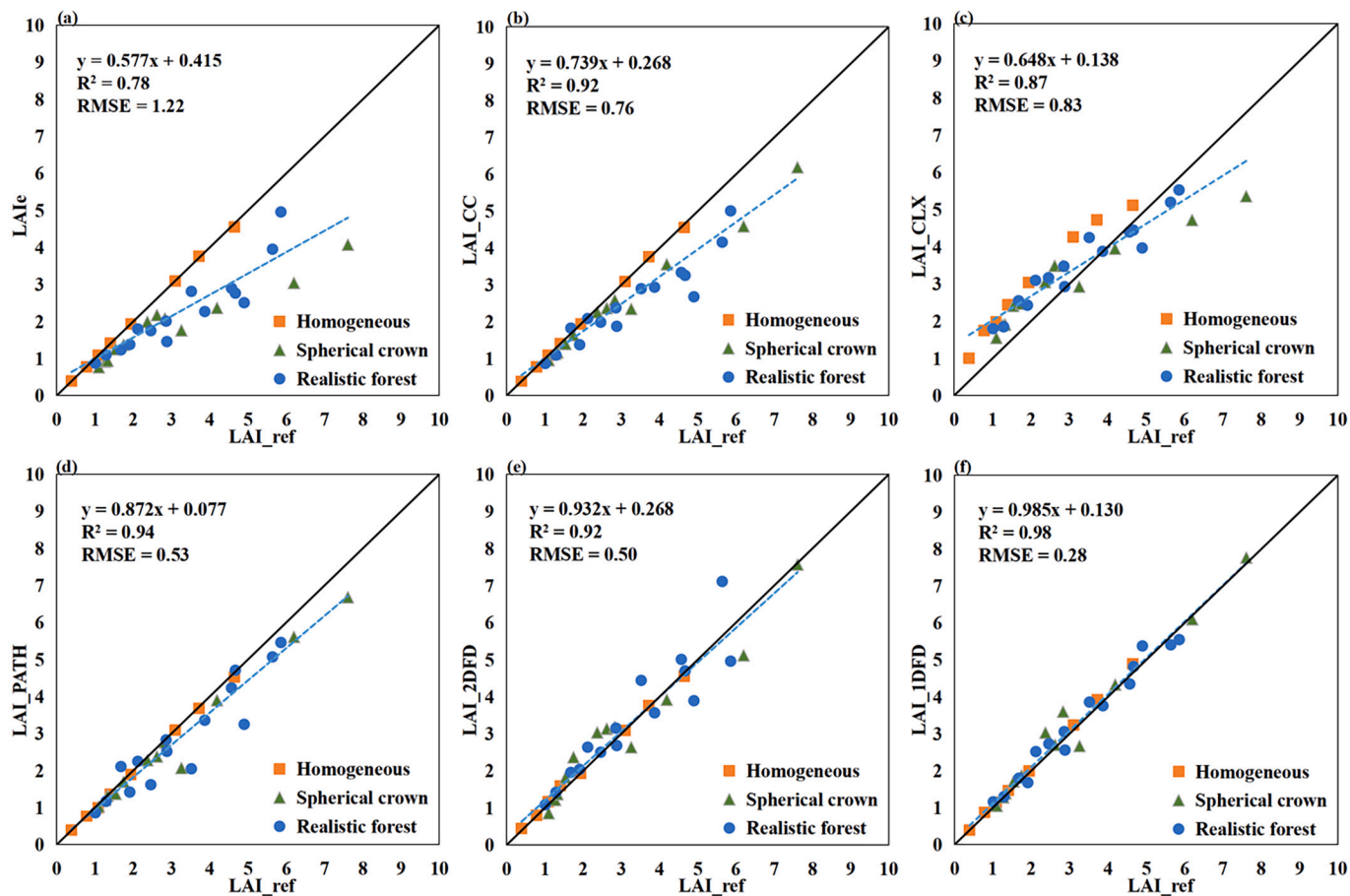


Fig. 6. All results were validated against the true LAI (LAI_{ref}). (a) LAI_e is the effective LAI of the simulated circular leaf scenes. Other results included those for the (b) CC, (c) CLX, (d) PATH, (e) 2D FD, and (f) 1DFD methods in simulated circular leaf scenes. The blue dashed line represents the linear regression, and the solid black line represents the 1:1 line. (For interpretation of the references to colour in this figure legend, the reader is referred to the web version of this article.)

LAI_{ref} for all the heterogeneous scenes.

Compared to the LAI_e, LAI_{CC} was closer to LAI_{ref}, but underestimation was still remained, especially for heterogeneous scenes with LAI_{ref} > 3. The RD of the CC method ranged from -45.3% to 1.3%, and the RMSE was 0.76.

The LAI_{CLX} overestimated LAI_{ref} in all homogeneous scenes and in heterogeneous scenes with LAI < 3. The LAI_{CLX} also showed a certain degree of underestimation in heterogeneous scenes with LAI > 4. The RD of the CLX method ranged from -29.6% to 156.4%, and the RMSE was 0.83.

Compared with the CC and CLX methods, the PATH method achieved better results. However, the PATH method underestimated the LAI of some heterogeneous scenes. The R² and RMSE equaled 0.94 and 0.53, respectively. The RD of the PATH method ranged from -36.5% to 25.6%.

The 2DFD method was the only one of the five comparable methods to use 2D information derived from the DCP images. The RD of the 2DFD method ranged from -22.1% to 35.2%, and the RMSE was 0.50. The LAI_{2DFD} was in good agreement with LAI_{ref} when the LAI for the scenes was < 4. However, the LAI_{2DFD} deviated from LAI_{ref} for scenes with LAI > 4.

The regression line between LAI_{1DFD} calculated using Eq. (13) and LAI_{ref} was close to the 1:1 line. The RD of the 1DFD method ranged from -18.1% to 27.8%. The LAI_{1DFD} was consistent with the LAI_{ref} for homogeneous scenes and did not systematically underestimate or overestimate the LAI_{ref} when LAI varied from 0.39 to 7.61. Overall, the 1DFD method performed the best (RMSE = 0.28, R² = 0.98). Results

from these simulated scenes indicated adding 1D FD information better corrected for the clumping effect.

4.1.2. Non-circular leaf scenes

In Section 2.2, the leaf was assumed to be circular when calculating the l_c . In fact, leaves have various shapes, and the assumption of the circular shape likely causes errors in the calculation results. Therefore, vegetation scenes with non-circular leaves were simulated (see Section 3.1) to test the accuracy of the 1DFD method (Fig. 7). As with the circular leaf scenes, the LAI_{1DFD} was the most accurate (RMSE = 0.37, R² = 0.94). Results for the CC, CLX, PATH, and 2DFD methods were also similar to those for circular leaf scenes (Fig. 6). For example, LAI_{CC} values were lower than LAI_{ref} for heterogeneous scenes. The LAI_{CLX} and LAI_{PATH} were lower than LAI_{ref} for heterogeneous scenes with LAI_{ref} > 3. Finally, the 2DFD method overestimated (e.g., LAI_{ref} = 4.13) or underestimated (e.g., LAI_{ref} = 5.52) LAI for scenes with LAI_{ref} > 3. The RD of 2DFD method ranged from -46.4% to 21.9%.

The 1DFD method provided good estimates of LAI for scenes with non-circular leaves (Fig. 7). This may result from the fact that the length of the FD segment was set to ten times the leaf radius, which reduced the impact of foliage shape and better reflected information about the distribution of the leaf chords along the transect.

4.1.3. RAMI actual canopy scenes

The LAI_e and LAI estimates for the four RAMI actual canopy scenes are shown in Fig. 8. As illustrated in Fig. 8, the CC method still intensively underestimated the LAI of the four RAMI scenes, and the RD

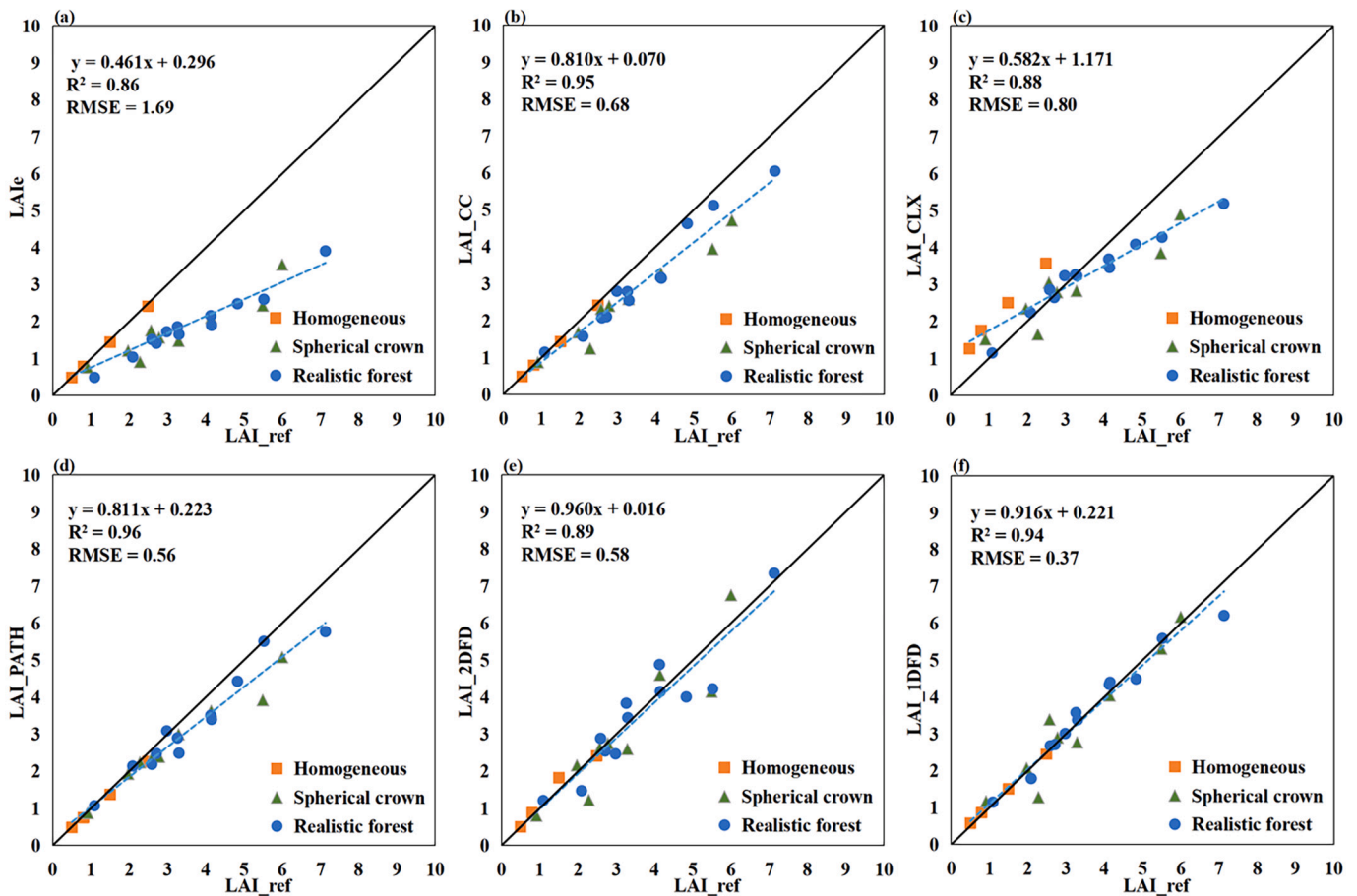


Fig. 7. Validation of the effect of leaf shape on estimates of LAI where (a) LAI_e is the effective LAI. (b) LAI_{CC}, (c) LAI_{CLX}, (d) LAI_{PATH}, and (e) LAI_{2DFD}, and (f) LAI_{1DFD} represent LAI estimated by CC, CLX, PATH, 2DFD, and 1DFD methods for non-circular leaf scenes, respectively. The blue dashed line represents the linear regression, and the solid black line represents the 1:1 line. (For interpretation of the references to colour in this figure legend, the reader is referred to the web version of this article.)

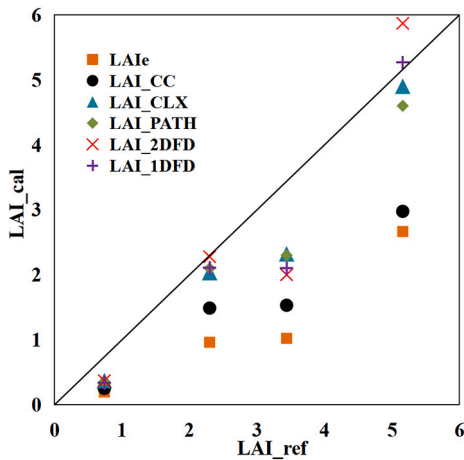


Fig. 8. Results of four RAMI actual canopy scenes. LAI_cal and LAI_ref are the calculated LAI and true LAI, respectively. LAI_e is the effective LAI. LAI_{CC}, LAI_{CLX}, LAI_{PATH}, LAI_{2DFD}, and LAI_{1DFD} represent LAI estimated by CC, CLX, PATH, 2DFD, and 1DFD methods, respectively. The solid black line represents the 1:1 line.

ranged from -65.6% to -35.2%. The CLX, PATH, 2D FD, and 1DFD methods obtained similar results. The RD of the CLX, PATH, 2DFD, and 1DFD methods ranged from -49.6% to -5.0%, from -51.2% to -8.7%, from -49.6% to 13.8%, and from -54.1% to 2.1%, respectively. These methods could well correct the clumping effect of most scenes, but due to the complex structure of the canopy and the influence of various components (i.e., leaves and branches), the calculated LAI still deviated from the true values, especially for the Järvelsjä Birch Stand (LAI_{ref} = 3.44).

4.2. LAI estimates in apricot orchard scenes using UAV imagery and TRAC data

For each orchard plot, the LAI results and LAI_e of UAV images and TRAC transects are presented in Fig. 9. The LAI calculated using the same methods with different types of data was different. The difference may be caused by different viewing angles and sampling representativeness between TRAC and UAV images. Taking plot 2 as an example, the $P(\theta)$ of TRAC data was 0.35, while that of UAV image was 0.51.

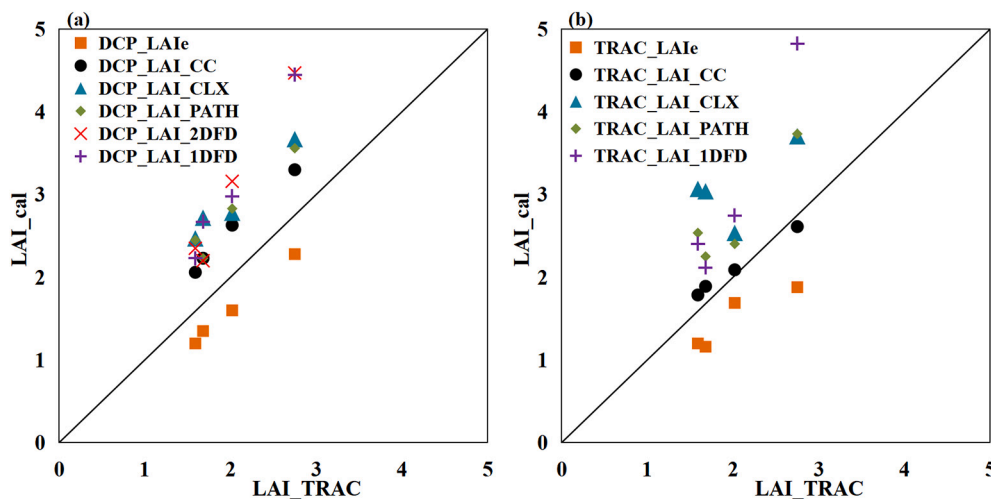


Fig. 9. Validation of LAI retrieval using (a) UAV DCP images and (b) TRAC data measured in the apricot orchards. LAI_cal and LAI_{TRAC} are the calculated LAI and measured LAI using TRAC instrument, respectively. LAI_e is the effective LAI. X_{LAI}Y (e.g., DCP_LAI_{CC}) represents LAI estimated using method Y (i.e., CC, CLX, PATH, 2D FD, or 1DFD method) with data X (i.e., UAV DCP images or TRAC transects). The solid black line represents the 1:1 line.

Moreover, the value of $G(\theta)$ also varied with the viewing angle.

The LAI results calculated using the CC method (DCP_LAI_{CC} and TRAC_LAI_{CC} in Fig. 9) were the most consistent with LAI measured by TRAC (LAI_{TRAC}) because measurements taken with the TRAC instrument were based on the CC method. The trend in LAI results calculated by these five methods for measured data was roughly the same as that for the simulated data. In addition, the LAI results calculated using the 1DFD method (DCP_LAI_{1DFD} and TRAC_LAI_{1DFD}) were higher than LAI_{TRAC}. This could result from the fact that the TRAC instrument estimates were based on those of the CC method and may not be able to fully correct for within-crown clumping. This may cause the LAI measured by the TRAC to be lower than the true LAI.

4.3. LAI estimates for conifer forest scenes using upward-facing DCP images, DHP images, and TRAC transects

4.3.1. Comparison of LAI estimation methods for conifer forest scenes

For each coniferous forest plot, the LAI results of five methods and LAI_e are presented in Fig. 10. Due to the clumping effect, LAI_e was significantly lower than the litter collection value (LAI_{litter}). The RD of LAI_e for DCP images, DHP images, and TRAC transects ranged from -44.4% to -69.0%, from -31.6% to -64.8%, and from -26.7% to -3.0%, respectively. The underestimation of LAI was approximately 70% for plot 6 (LAI_{litter} = 3.58), which indicated that the CI should be about 0.3. The heterogeneity of plot 6 was higher than other plots because it had the lowest stand density and smallest FVC (stand density = 384 stems / ha, FVC = 0.43 in Table 6) but large LAI (LAI_{litter} = 3.58). Therefore, it was challenging to select reasonable sampling points for photography measurement in plot 6, particularly considering the limited field of view of DCP images. Although both the woody-to-total area ratios of plots 5 and 6 were 0.16 (Table 7), there were far fewer woody components in the images taken in plot 6 than in those taken in the plot 5. This phenomenon indicated the insufficient number of samplings for plot 6 and explained why the LAI was greatly underestimated for this plot, even after being corrected by the five methods. Therefore, the following analysis excluded plot 6.

4.3.2. DCP images and DHP images

The CC method showed improved results by correcting the clumping effect caused by large gaps between crowns. But the underestimation still remained because of within-crown clumping. The RD of CC method ranged from -42.4% to -29.3% for DCP images and from -31.0% to

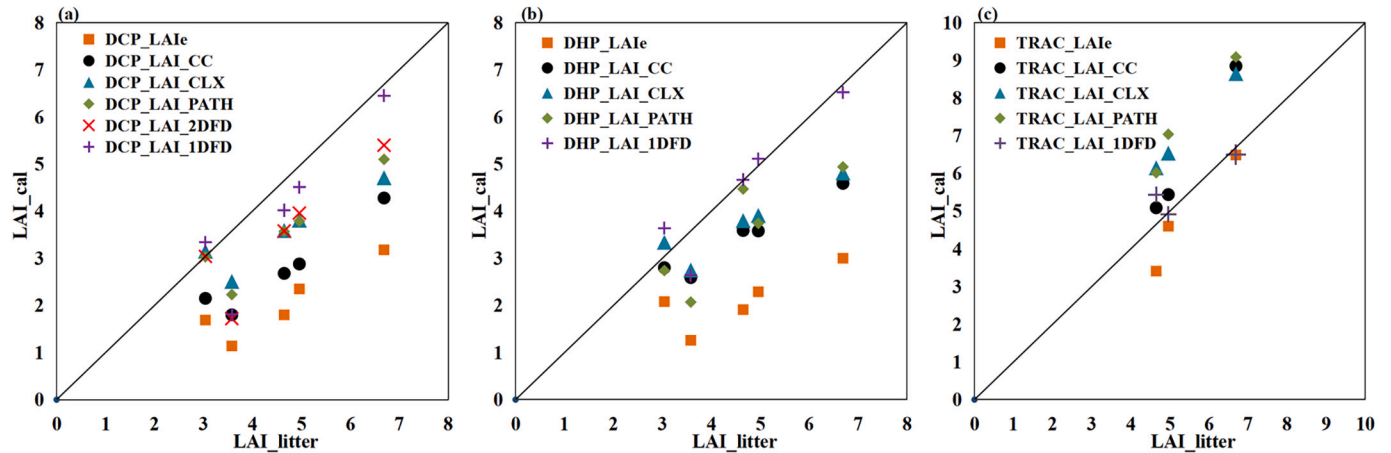


Fig. 10. Comparison between calculated LAI (LAI_cal) and litter collection values (LAI_litter) in coniferous forest plots. (a), (b), and (c) are the results of DCP images, DHP images, and TRAC transects, respectively. LAI_e is the effective LAI. X_{LAI}Y (e.g., DCP_LAI_CC) represents LAI estimated using method Y (i.e., CC method, CLX method, PATH method, 2DFD method, or 1DFD method) with data X (i.e., DCP images, DHP images, or TRAC transects). The solid black line represents the 1:1 line.

Table 6
Field measurement data for plots in Huailai.

Plot	1	2	3	4
Tree type	Apricot			
Mean tree height (m)	3.36	2.57	2.57	3.11
Average crown width (m)	3.38	2.99	2.99	3.23
Row spacing (m)	3.38	2.05	—*	—*
Photography date	July 30 and 31, 2019			May 10, 2021
Size (m)	30 × 30			
Number of selected photos	10			
Flight altitude (m)	30			
Image dimension (pixel × pixel)	4000 × 3000			

* Row spacing for plots 3 and 4 was not measured.

Table 7
Field measurement data for plots in Chengde (Zou et al., 2018).

Plot	5	6	7	8	9
Mean tree height (m)	19.43	20.4	12.58	13.31	8.73
Average DBH (cm)	26.58	27.22	12.71	14.14	9.23
Mean element width (mm)	21.66	23.34	17.91	21.09	17.60
Stand density (stems/ha)	464	384	2320	1760	3904
Tree age (years)	54	55	21	22	13
Needle-to-shoot area ratio	1.30	1.17	1.14	1.17	1.28
Woody-to-total area ratio	0.16	0.16	0.20	0.24	0.23
Fractional vegetation cover of the plot	0.52	0.43	0.74	0.63	0.82
Litter collection LAI	4.65	3.58	4.96	3.04	6.69
Tree species	<i>Larix principis-rupprechtii</i> Mayr				
Number of photos	16				
Image dimension (pixel × pixel)	5472 × 3648 (DCP), 5472 × 3678 (DHP)				

−7.9% for DHP images. This supported the idea that the CC method can properly account for clumping caused by large gaps between crowns, but it cannot completely correct for clumping within the crown (Hu et al., 2014; Yan et al., 2016), e.g., the clumping caused by the crown shape (Jiang et al., 2021).

The CLX method more effectively modified the results than the CC method, as demonstrated by the fact that the RD ranged from −29.6% to −3.6% for DCP images and from −28.0% to 9.9% for DHP images. However, the CLX method underestimated LAI_{ref} in heterogeneous scenes with large LAI values (i.e., LAI > 3).

The PATH method performed better compared to the CC and CLX methods. The LAI_{PATH} of plots 5 and 8 were nearly identical to the LAI_{litter} of plots 5 and 8, respectively. However, the RD of PATH

method for other plots ranged from −23.8% to −23.2% for DCP images and from −24.6% to −9.9% for DHP images. This may be related to the fact that the PATH method assumed leaves are randomly distributed in the sliding windows used to calculate the path length distribution along the transect (Hu et al., 2014), but the leaves within the sliding windows will probably be clumped in practice. This assumption may result in underestimation of LAI using the PATH method.

Since the 2DFD method could not be used for DHP images, only the LAI of DCP images was estimated. The results from the 2DFD method were similar to those of the PATH method, achieving similar results for plot 8 but underestimating the LAI of other plots (RD ranged from −23.0% to −19.3%). This may be because the 2DFD method used a box nearly ten times the leaf area in the calculation of FD using the BCM. In scenes with large LAI and low gap probability, the spatial distribution information of some small gaps was ignored, which had an impact on the calculation of FD.

The LAI_{1DFD} showed the highest accuracy with an RD ranging from −13.5% to 9.9% for DCP images and from −3.0% to 19.7% for DHP images. This indicated the 1DFD method could properly correct for clumping. The RDs of DCP were more centered at 0 than those of DHP. This may be due to the fact that the pixels of the DHP image used for LAI calculation (i.e., observations with the zenith angle being 55°–60°) had more mixed pixels than the DCP image, which affected the calculation of gap probability and LAI. Assuming a constant $G(\theta)$ of 0.5 possibly caused the deviation of the LAI estimates from the true values for DCP images, as the coniferous species in this study exhibited low $G(\theta)$ at the nadir view (Yan et al., 2021).

4.3.3. TRAC transects

The LAI_e for TRAC transects (TRAC_LAI_e in Fig. 10 (c)) was quite different from that for DCP images and DHP images (DCP_LAI_e and DHP_LAI_e in Figs. 10 (a) and (b)). Except for plot 5 (LAI_{litter} = 4.65), the TRAC_LAI_e was almost the same as the LAI_{litter}. The difference of the LAI_e was mainly caused by the difference of the $P(\theta)$ measured by the instruments. The $P(\theta)$ for plots 5, 7, and 9 measured by DCP and DHP ranged from 0.20 to 0.41 and from 0.06 to 0.20, respectively, while the $P(\theta)$ measured by TRAC ranged from 0.01 to 0.07. Other studies also indicated that the $P(\theta)$ measured by TRAC was smaller than that measured by other instruments (Pisek et al., 2011a). The CLX and PATH methods applied the Beer-Lambert Law on sub-segments which were 10 times (20 times) the leaf width for CLX (PATH) method. However, the sub-segments extracted from the TRAC transects with small $P(\theta)$ were likely to do not contain gaps. Accordingly, a half-pixel size gap was manually added in the segments in the CLX method to avoid calculating

the logarithm of zero (Leblanc et al., 2005). Similarly, the PATH method avoided calculating the logarithm of zero by increasing the segment length until the segment contained a gap (Hu et al., 2014). These may be the reasons for the overestimation of the LAI for plots 5, 7, and 9 retrieved by the CLX and PATH methods (Fig. 10 (c)). Instead, the 1DFD method did not significantly overestimate the LAI. The calculated FD and CI by the 1DFD method were close to 1 for plots 7 and 9, where the TRAC_LAI_e was close to the LAI_{litter}, indicating that the 1DFD method correctly reflected the clumping information of leaves.

4.4. The analysis of influential factors for 1DFD method

4.4.1. Impact of the FD segment length for the 1DFD method

The FD segment length was set to 10 times the leaf radius (i.e., $s = 10r$) in Section 2.1. This trade-off choice was based on other research (Bernston and Stoll, 1997; Foroutan-pour et al., 1999a). To verify the rationality of this choice, we calculated the results of the simulated scenes with circular leaves when $s = r$ (called 1DFD_{1r} method), $s = 5r$ (1DFD_{5r} method), and $s = 20r$ (1DFD_{20r} method). The results are shown in Fig. 11. When the s was one, five, and 20 times the r , the calculated LAI for homogenous scenes was higher than the LAI_{ref}. The 1DFD_{1r} method underestimated the LAI of most heterogenous scenes, the RD for heterogenous scenes was -50.8% to 7.0% . Controversially, the 1DFD_{20r} method overestimated the LAI of most heterogenous scenes, the RD for heterogenous scenes was -32.4% to 71.3% . Although the 1DFD_{5r} method achieved better results (RMSE = 0.60, $R^2 = 0.89$), the calculated LAI was still biased compared to the reference LAI, and the RD was -36.8% to 25.8% .

If a short FD segment (e.g., $s = r$) intersected a leaf chord, the next FD segment was likely to intersect the same leaf chord, which did not satisfy the assumption in Eq. (2). Moreover, the calculated FD may reflect the leaf shape information. However, the number of long FD segments (e.g., $s = 20r$) on each transect was small, which affected the calculation accuracy of the FD as a statistical indicator. In addition, FD calculated using long FD segments primarily reflect information at crown scale. Therefore, using the 10 times leaf radius as the FD segment length was reasonable and recommended based on our experiments.

4.4.2. Effect of leaf projection function

The $G(\theta)$ was usually assumed to be 0.5 if it was not measured during a field campaign (Leblanc and Chen, 2001; Pisek et al., 2011a; Pisek et al., 2011b; Walter et al., 2003). This assumption was also adopted in this study. The four RAMI actual canopies introduced in Section 3.2 were used to assess the impact of this assumption on the LAI retrieval. The LAI_e and LAI values estimated by the five method in comparison are

presented in Fig. 12. There were differences between the LAI values calculated with the correct $G(0)$ (the blue histograms in Fig. 12) and the LAI values calculated assuming $G(0) = 0.5$ (called the LAI_{0.5} hereafter; the red histograms in Fig. 12). If the reference $G(0)$ was less (greater) than 0.5, the LAI_{0.5} was smaller (greater) than the LAI calculated with the correct $G(0)$. Among the five methods in comparison, the LAI calculated by the 2DFD method had the smallest change, followed by the CC method and PATH method, while the 1DFD method and CLX method had larger changes. Therefore, if the observation direction is far from 57° , it is better to measure a relatively accurate $G(\theta)$ during a field campaign, particularly considering the limited field of view encountered in DCP images.

4.4.3. Effect of DCP image resolution on estimation accuracy

There will be more mixed pixels in images with low resolution, which reduces image classification accuracy, thus affecting the accuracy of both FD and LAI_e estimates. Three ortho DCP images with different resolutions were generated for four realistic forest canopy scenes to assess the effect of image resolution. The resolutions of the three images were 5.0 cm, 1.0 cm and 0.5 cm respectively, and corresponded to 1-, 5- and 10-pixel wide leaf radiuses, respectively.

The calculated $P(0)$, 1D FD, and 2D FD were shown in Table 9. Except for the resolution of 5.0 cm, the $P(0)$ calculated at 1.0 cm and 0.5 cm resolutions were generally the same. The difference of the LAI_e caused by the different $P(0)$ ranged from 0.05 to 0.96. The differences of the 1D FD and 2D FD for various resolutions were from 0.00 to 0.04 and from 0.00 to 0.02, respectively.

The estimated LAI values using these images at different resolutions are presented in Fig. 13. The results obtained by the CLX method at different resolutions had better stability (Fig. 13 (b)), with the difference of LAI acquired from the images of different resolutions from 0.00 to 0.39. In contrast, the LAI values calculated using the CC, PATH, 2DFD and 1DFD methods at 5.0 cm resolution (leaf radius equaled 1-pixel) were significantly larger than that calculated at other resolutions, and the differences of LAI between images of different resolutions calculated by these methods ranged from 0.00 to 1.34, from 0.05 to 1.35, from 0.00 to 1.73 and from 0.12 to 2.34, respectively. However, there were good agreements between LAI_{1DFD} and LAI_{ref} at 0.5 cm and 1 cm resolutions. The difference between LAI_{1DFD} and LAI_{ref} for each scene with 0.5 cm and 1 cm resolutions ranged from 0.00 to 0.48.

The FD methods were sensitive to the image resolution when the leaf radius equaled 1-pixel, because the image resolution affected the $P(0)$, FD (Table 9), and the calculation of CI and LAI (Eq. (13)). This indicated that image resolution should be considered when using the FD methods. The number of pixels occupied by the radius of a leaf or shoot is

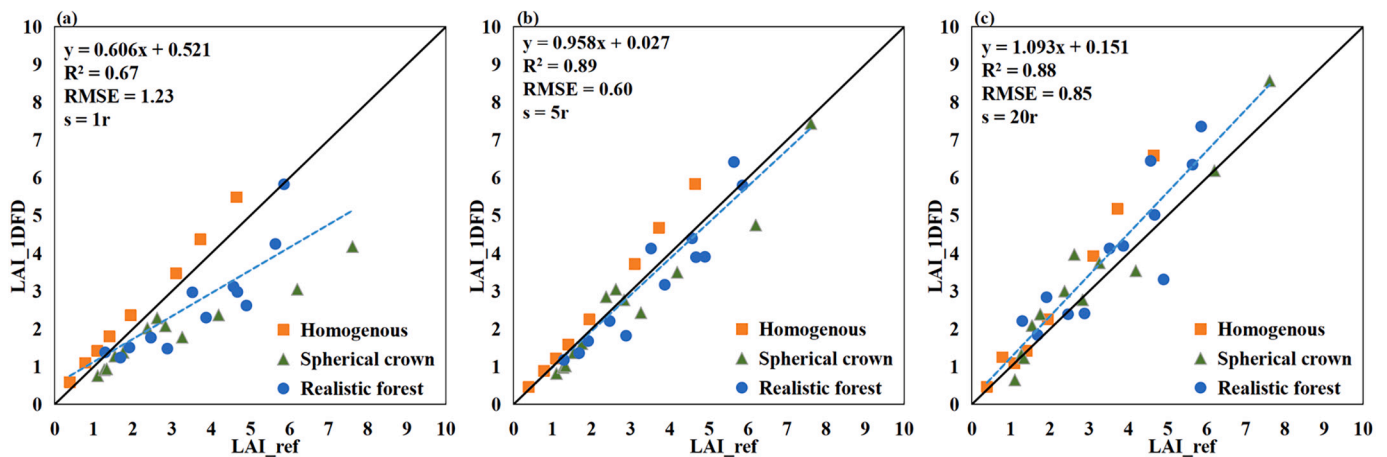


Fig. 11. (a), (b), and (c) are the results of simulated circular leaf scenes when FD segment length is one, five, and 20 times the leaf radius, respectively. LAI_{ref} indicates the true LAI, and LAI_{1DFD} is the LAI calculated using the 1DFD method. The solid black line represents the 1:1 line.

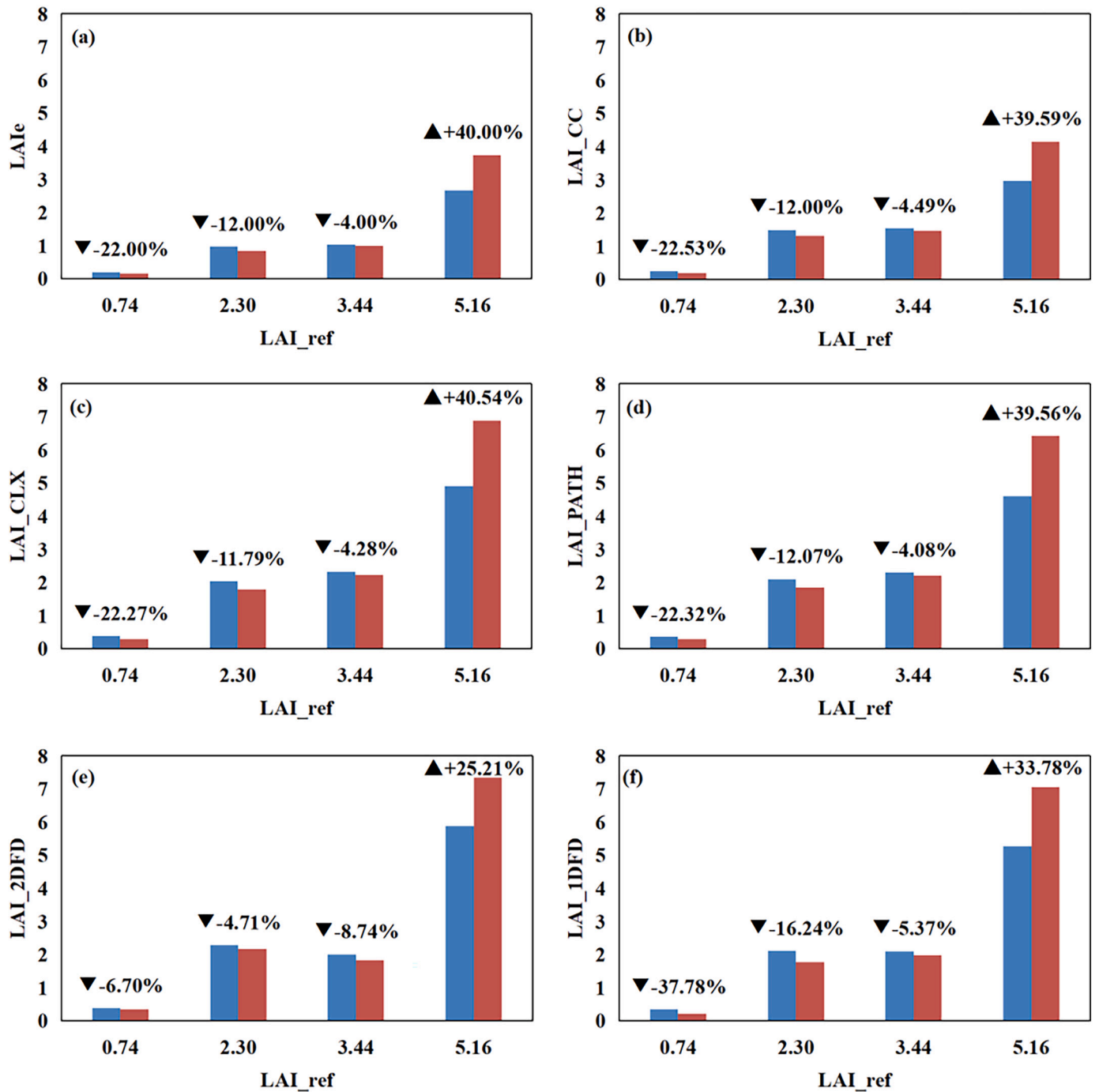


Fig. 12. Effect of unknown leaf projection function at nadir direction ($G(0)$) for (a) LAI_e, (b) CC, (c) CLX, (d) PATH, (e) 2DFD, and (f) 1DFD methods. The LAI values calculated with the correct $G(0)$ (called LAI_r) corresponded to the blue histograms, while the LAI value calculated assuming $G(0) = 0.5$ (called LAI_{0.5}) corresponded to the red histograms. The abscissa was the reference LAI. The percentiles in (a)-(f) represent $\frac{LAI_{0.5} - LAI_r}{LAI_r} \times 100\%$.

recommended to be at least 5 (*i.e.*, $r \geq 5$). Numerous segmentation methods were developed for upward-looking DCP images whereas the image segmentation for downward-looking DCP was more difficult due to the complex background. Method that accounts for the shadow effect would be a priority.

4.5. Comparison of 1D FD to other LAI measurement methods

The 2DFD method is recently proposed and attempts to correct for the clumping effect by introducing 2D FD information from the DCP image (Li and Mu, 2021). It does not assume a distribution pattern of

leaves in space and can correct for clumping at different scales. However, the 2DFD method cannot be used with transects measured by a TRAC or extracted from DHP images. The 1DFD method proposed herein uses 1D FD information to comprehensively correct for the clumping effect. The high consistency between reference LAI and LAI calculated from the 1DFD method in simulated scenes (Fig. 6 (f) and Fig. 7 (f)) indicates that this method produces reasonable results that are generally more accurate than current methods.

As a 1D method, the 1DFD method does not face the difficulties of the traditional 1D methods (LX, CC, and CLX methods). The 1DFD method applies sub-segment (FD segment) when calculating 1D FD, yet it does

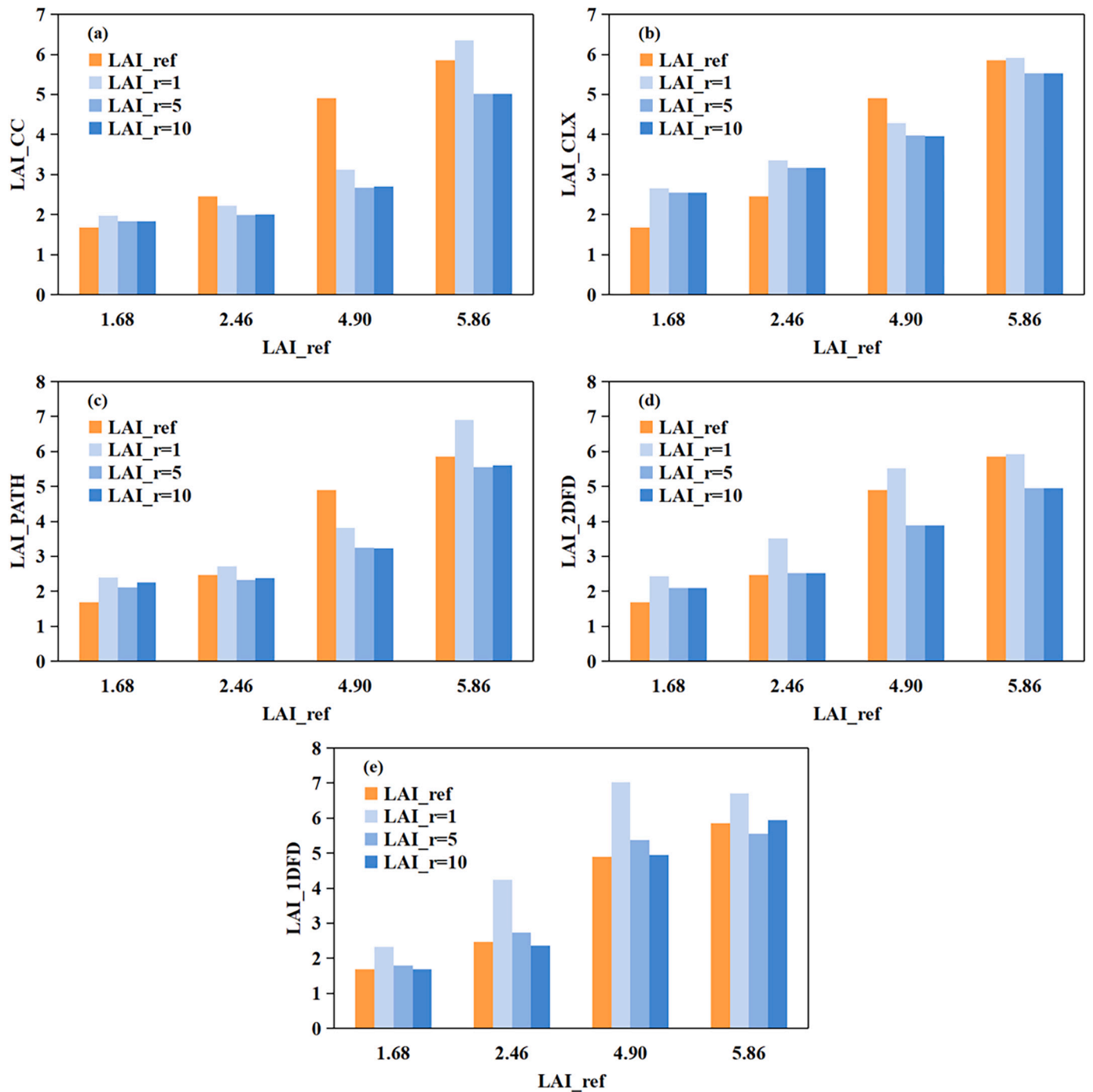


Fig. 13. Image resolution effect on estimation results for the (a) CC, (b) CLX, (c) PATH, (d) 2DFD, and (e) 1DFD methods. The LAI_ref refers to the reference LAI, while LAI_r = 1, LAI_r = 5, and LAI_r = 10 represent the LAI obtained when the leaf radius (5 cm) equals 1-, 5- or 10-pixel width, respectively.

not assume that the leaves are randomly distributed in the sub-segment. Moreover, this method applies the Beer-Lambert Law along the entire transect rather than on each FD segment. Generally, transects from DCP images, DHP images, or TRAC measurement are thousands of times the leaf width and are more likely to contain gaps than sub-segment that are only 10 times the leaf width. Therefore, the 1DFD method is less likely to face calculating the logarithm of 0 than LX and CLX methods.

Compared to the 2DFD method, the 1DFD method is applicable to DHP and TRAC instruments and is more accurate for dense canopies (LAI > 3 in Figs. 6 and 7). The 1DFD method extracts transects from images and then calculates the FD of these transects, generating more samples from an image when compared to the 2DFD method. Therefore,

the FD calculated from the 1DFD method can more accurately reflect distribution information of leaves and small gaps in the image for high-LAI scenes. For example, the 2D FD of the Realistic forest scene is 2.00 with LAI = 5.86 (Table 8), which should be less than the 2D FD of a scene of randomly distributed leaves (leaves filled in a 2D space). In contrast, the 1D FD of some transects of this scene is around 1.00 which is the same as the 1D FD for a transect of the randomly distributed leaves, while the 1D FD of other transects in this scene is around 0.90. Therefore, the value of LAI_1DFD (5.55) is more accurate than LAI_2DFD (4.96).

However, the 1DFD method does not outperforms 2DFD method in all aspects as the 2DFD method considers 2D spatial correlation yet the

Table 8

The true LAI (LAI_ref), P(0), CI, 1D FD, and 2D FD of the simulated circular leaf scenes. “1D FD” in the table was the average of the 1D FD of each row of the image.

LAI_ref	Homogenous scenes					Discrete spherical crown scenes					Realistic forest scenes				
	0.78	1.09	1.94	3.10	4.65	1.10	1.54	2.62	6.20	7.61	1.01	1.29	2.86	4.67	5.86
P(0)	0.68	0.58	0.38	0.21	0.10	0.68	0.53	0.34	0.22	0.13	0.65	0.58	0.36	0.25	0.08
CI	0.99	1.00	1.00	1.01	0.99	0.70	0.82	0.82	0.49	0.54	0.85	0.84	0.71	0.59	0.86
1D FD	0.91	0.98	1.00	1.00	1.00	0.77	0.90	0.97	0.96	0.97	0.88	0.92	0.94	0.96	0.99
2D FD	1.89	1.96	2.00	1.99	2.00	1.85	1.93	1.97	1.97	1.98	1.87	1.92	1.92	1.96	2.00

Table 9

The gap probability at nadir view (P(0)), 1D FD, and 2D FD of DCP images at different resolutions (i.e., 0.50 cm, 1.00 cm, and 5.00 cm) for four simulated scenes. The “R” refers to the resolution in centimeters. “1D FD” in the table is the average of the 1D FD of each row of an image.

LAI	1.68			2.46			4.90			5.86		
R (cm)	0.50	1.00	5.00	0.50	1.00	5.00	0.50	1.00	5.00	0.50	1.00	5.00
P(0)	0.54	0.54	0.53	0.42	0.42	0.39	0.29	0.29	0.25	0.08	0.08	0.05
1D FD	0.84	0.88	0.88	0.90	0.92	0.90	0.91	0.95	0.95	0.99	0.99	0.98
2D FD	1.88	1.88	1.86	1.92	1.92	1.91	1.96	1.97	1.96	2.00	2.00	2.00

1DFD method doesn't. For example, users should be careful to extract 1D transects from downward-looking images for row structure scenes. Transects parallel and perpendicular to the row direction would result in quite different LAI estimates for the 1DFD method.

Like other methods based on the Beer-Lambert law (LX, CC, CLX, PATH and 2DFD methods), the 1DFD method is affected by the calculation accuracy of the gap probability and leaf projection function. The retrieval accuracy of LAI depends on the settings of spatial resolution, the field of view and sampling footprint if the DCP manner is used. The 1DFD method and other indirect methods cannot consider the woody component effect and the clumping within shoots when used for coniferous canopies. Therefore, two additional parameters, woody-to-total area ratio and needle-to-shoot area ratio, need to be introduced to correct for the influences of woody components and the within shoot clumping, respectively.

5. Conclusions

Traditional methods for correcting clumping, which use gap information, have been widely used for decades to obtain leaf area index (LAI). To meet the requirements of high accuracy and new applications, additional information is needed to more comprehensively correct for clumping and obtain more accurate LAI. We propose a new method using one-dimensional fractal dimension (1D FD) to correct for the clumping effect and obtain accurate LAI. The relationship between 1D FD, LAI, and the clumping index (CI) is based on the box-counting method (BCM) and a binomial distribution model.

Simulated and field measurement data were used to validate the predictability and accuracy of the 1DFD method. The results obtained from simulated scenes show that the LAI estimated using the 1DFD method from digital cover photography (DCP) images achieves the best agreement with a reference LAI (RMSE = 0.28 and R² = 0.98 for circular leaf scenes; RMSE = 0.37 and R² = 0.94 for non-circular leaf scenes) and indicate the proposed method can correct the clumping effect more comprehensively than existing methods. When compared with the LAI measured using a tracing the radiation and architecture of canopies (TRAC), the 1DFD method produces good estimates of LAI for plots in

Appendix A. Number of leaf chords on a transect (N_C)

An image with an area A is the result of all leaves within the sampling range of the camera projected along the viewing direction. Given the assumption of horizontal and random distribution of leaves, whether a leaf in an image intersects with a transect is independent of other leaves, and the probability of each leaf intersecting with the transect is the same, thus fulfilling the requirement for binomial distribution. The number of leaf chords on a transect (N_C) equals to the number of leaves intersecting the transect. Therefore, N_C results from calculating its binomial distribution: N_C =

apricot orchards. For coniferous forest plots, the LAI estimated using the 1DFD method generally shows the most consistency with the LAI calculated using litter collection as compared to four similar methods whether using DCP images, digital hemispherical photography (DHP) images, or TRAC measurements. The 1DFD method improves on existing estimates of the LAI and may provide accurate LAI measurements for LAI product validation. This method has been compiled into a free software called FD_LAI, which can be found at https://github.com/CloudyCUG/FD_LAI.

Credit author statement.

Yongkang Lai: Conceptualization, Investigation, Methodology, Formal analysis, Writing - Original Draft; **Xihan Mu:** Conceptualization, Methodology, Writing - Review & Editing, Funding acquisition; **Weihua Li:** Writing - Review & Editing; **Jie Zou:** Resources, Writing - Review & Editing; **Yuequn Bian:** Investigation, Writing - Review & Editing; **Kun Zhou:** Resources; **Ronghai Hu:** Writing - Review & Editing; **Linyuan Li:** Writing - Review & Editing; **Donghui Xie:** Supervision, Writing - Review & Editing; **Guangjian Yan:** Supervision, Writing - Review & Editing, Funding acquisition.

Declaration of Competing Interest

The authors declare that they have no known competing financial interests or personal relationships that could have appeared to influence the work reported in this paper.

Data availability

Data will be made available on request.

Acknowledgements

This research is financially supported by the National Natural Science Foundation of China (Grant No. 42090013 and 41871230). Appreciation is sincerely expressed to the people who helped the field experiment: Yi Li and Xinli Liu from Beijing Normal University.

$N_L P_l$, where N_L is the total number of leaves in the image, P_l is the probability of a leaf in the image intersecting the transect. Without loss of generality, P_l equals the probability that a leaf randomly placed on a plane of area A (equals the image area) intersects with a fixed transect of length l (Fig. 1) (Miller and Norman, 1971):

$$P_l = \frac{lw + \sigma}{A} \tag{A1}$$

where σ is the leaf area of a single leaf, w is the leaf width, and $lw + \sigma$ is the maximum moving area of the leaf when it intersects with the transect (Fig. A1). Therefore, N_C can be expressed as:

$$N_C = N_L \frac{lw + \sigma}{A} \tag{A2}$$

When the leaf shape is assumed to be circular, σ equals πr^2 and w equals $2r$, where r is the radius of the leaf.

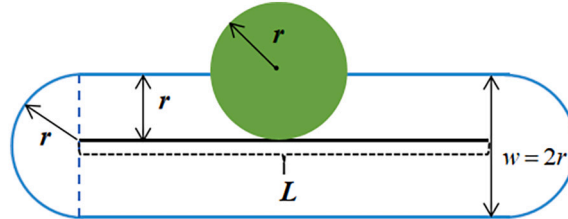


Fig. A1. Maximum moving area of the center of a leaf when the leaf intersects with the transect. The green circle represents a leaf and the segment in black shows the transect. The area enclosed by blue lines is the movable range of the leaf center when the leaf intersects the transect, and the area is $lw + \sigma$, where $\sigma = \pi r^2$ and r is the radius of the leaf. (For interpretation of the references to colour in this figure legend, the reader is referred to the web version of this article.)

Appendix B. Average length of all chords of a leaf (l_C)

The l_C is highly related to leaf shape. In this study leaves are considered circular. For a circular leaf, l_C is calculated as the integration of the distance from the leaf center to the transect (x) from 0 to r (Fig. B1):

$$l_C = \frac{1}{r} \int_0^r 2\sqrt{r^2 - x^2} dx = \frac{\pi r}{2} \tag{B1}$$

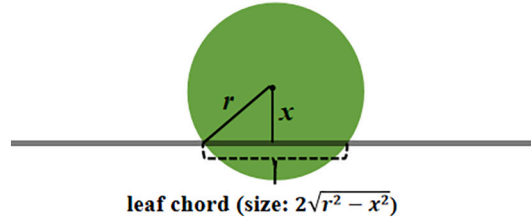


Fig. B1. The average length of all chords of the circular leaf (l_C) is calculated from a leaf with radius r (green circle) and its intersection with a transect (black line). The vertical distance from the leaf center to the transect is symbolized as x .

Appendix C. Relationship between 1D FD and LAI

The 1D FD of horizontally and randomly distributed leaves can be expressed as Eq. (6) (Eq. (C1)):

$$FD_d = 1 - \frac{s \cdot T Q^{T-1}}{l \cdot (1 - Q^T)} \tag{C1}$$

where $Q = 1 - \frac{\pi r + 2s}{2l}$ and $T = \frac{2rN_L l + N_L \pi r^2}{A}$. The term Q^T is:

$$Q^T = \left(1 - \frac{\pi r + 2s}{2l}\right)^{\frac{2N_L l}{A}} \cdot \left(1 - \frac{\pi r + 2s}{2l}\right)^{\frac{N_L \pi r^2}{A}}$$

Considering that transect length l is infinite relative to r and that $s = 10r$, then the term $\left(1 - \frac{\pi r + 2s}{2l}\right)^{\frac{2N_L l}{A}}$ is equal to e . Thus, Q^T is simplified as:

$$Q^T = e^{-\frac{N_L \pi r^2 + 20N_L r^2}{A}} \cdot \left(1 - \frac{\pi r + 20r}{2l}\right)^{\frac{N_L \pi r^2}{A}} \tag{C2}$$

Then, considering that $LAI = \frac{N_L \pi r^2}{A}$, Eq. (C2) can be transformed into:

$$Q^T = e^{-\left(\frac{LAI + 20LAI}{\pi}\right)} \cdot \left(1 - \frac{\pi r + 20r}{2l}\right)^{LAI} \tag{C3}$$

Similarly, term $s \bullet T$ in Eq. (C1) can be expressed as:

$$s \bullet T = \frac{20l \bullet LAI}{\pi} + 10r \bullet LAI \quad (C4)$$

Finally, combining Eqs. (C1), (C3), and (C4), we obtain the relationship (Eq. (C5)) between LAI and FD for horizontally and randomly distributed leaves (Eqs. (C5)–(C7) are the same as Eqs. (7)–(9), respectively):

$$FD_d = 1 - \frac{10LAI(2l + \pi r) \bullet H_d}{\pi l(1 - H_d \bullet V_d)} \quad (C5)$$

where

$$H_d = \exp\left(-LAI - \frac{20LAI}{\pi}\right) \bullet V_d^{LAI-1} \quad (C6)$$

and

$$V_d = 1 - \frac{\pi r + 20r}{2l} \quad (C7)$$

References

- Aldos, C.L., Escos, J., Emlen, J., Freeman, D., 1999. Characterization of branch complexity by fractal analyses. *Int. J. Plant Sci.* 160, S147–S155.
- Asner, G.P., Scurlock, J.M., Hicke, A., J., 2003. Global synthesis of leaf area index observations: implications for ecological and remote sensing studies. *Glob. Ecol. Biogeogr.* 12, 191–205.
- Baret, F., de Solan, B., Lopez-Lozano, R., Ma, K., Weiss, M., 2010. GAI estimates of row crops from downward looking digital photos taken perpendicular to rows at 57.5 zenith angle: theoretical considerations based on 3D architecture models and application to wheat crops. *Agric. For. Meteorol.* 150, 1393–1401.
- Berntson, G., Stoll, P., 1997. Correcting for finite spatial scales of self-similarity when calculating fractal dimensions of real-world structures. *Proc. R. Soc. Lond. Ser. B Biol. Sci.* 264, 1531–1537.
- Bisoi, A.K., Mishra, J., 2001. On calculation of fractal dimension of images. *Pattern Recogn. Lett.* 22, 631–637.
- Black, T.A., Chen, J.-M., Lee, X., Sagar, R.M., 1991. Characteristics of shortwave and longwave irradiances under a Douglas-fir forest stand. *Can. J. For. Res.* 21, 1020–1028.
- Breda, N.J., 2003. Ground-based measurements of leaf area index: a review of methods, instruments and current controversies. *J. Exp. Bot.* 54, 2403–2417.
- Calders, K., Origo, N., Burt, A., Disney, M., Nightingale, J., Raunonen, P., Åkerblom, M., Malhi, Y., Lewis, P., 2018a. Realistic forest stand reconstruction from terrestrial LiDAR for radiative transfer modelling. *Remote Sens.* 10, 933.
- Calders, K., Origo, N., Disney, M., Nightingale, J., Woodgate, W., Armston, J., Lewis, P., 2018b. Variability and bias in active and passive ground-based measurements of effective plant, wood and leaf area index. *Agric. For. Meteorol.* 252, 231–240.
- Chen, J., Black, T., 1991. Measuring leaf area index of plant canopies with branch architecture. *Agric. For. Meteorol.* 57, 1–12.
- Chen, J.M., Black, T., 1992. Defining leaf area index for non-flat leaves. *Plant Cell Environ.* 15, 421–429.
- Chen, J.M., Cihlar, J., 1995a. Plant canopy gap-size analysis theory for improving optical measurements of leaf-area index. *Appl. Opt.* 34, 6211–6222.
- Chen, J.M., Cihlar, J., 1995b. Quantifying the effect of canopy architecture on optical measurements of leaf area index using two gap size analysis methods. *IEEE Trans. Geosci. Remote Sens.* 33, 777–787.
- Chen, J.M., Rich, P.M., Gower, S.T., Norman, J.M., Plummer, S., 1997. Leaf area index of boreal forests: theory, techniques, and measurements. *J. Geophys. Res. Atmos.* 102, 29429–29443.
- Chianucci, F., Cutini, A., 2013. Estimation of canopy properties in deciduous forests with digital hemispherical and cover photography. *Agric. For. Meteorol.* 168, 130–139.
- Cohen, W.B., Maiersperger, T.K., Yang, Z., Gower, S.T., Turner, D.P., Ritts, W.D., Berterretche, M., Running, S.W., 2003. Comparisons of land cover and LAI estimates derived from ETM+ and MODIS for four sites in North America: a quality assessment of 2000/2001 provisional MODIS products. *Remote Sens. Environ.* 88, 233–255.
- Daughtry, C.S., 1990. Direct measurements of canopy structure. *Remote Sens. Rev.* 5, 45–60.
- Dufrène, E., Bréda, N., 1995. Estimation of deciduous forest leaf area index using direct and indirect methods. *Oecologia* 104, 156–162.
- Fang, H., 2021. Canopy clumping index (CI): a review of methods, characteristics, and applications. *Agric. For. Meteorol.* 303, 108374.
- Fang, H., Baret, F., Plummer, S., Schaeppman-Strub, G., 2019. An overview of global leaf area index (LAI): methods, products, validation, and applications. *Rev. Geophys.* 57, 739–799.
- Foroutan-pour, K., Dutilleul, P., Smith, D.L., 1999a. Advances in the implementation of the box-counting method of fractal dimension estimation. *Appl. Math. Comput.* 105, 195–210.
- Foroutan-pour, K., Dutilleul, P., Smith, D.L., 1999b. Soybean canopy development as affected by population density and intercropping with corn: fractal analysis in comparison with other quantitative approaches. *Crop Sci.* 39, 1784–1791.
- Foroutan-pour, K., Dutilleul, P., Smith, D.L., 2001. Inclusion of the fractal dimension of leafless plant structure in the Beer-Lambert law. *Agron. J.* 93, 333–338.
- Gonsamo, A., Pellikka, P., 2008. Methodology comparison for slope correction in canopy leaf area index estimation using hemispherical photography. *For. Ecol. Manag.* 256, 749–759.
- Gonsamo, A., Pellikka, P., 2009. The computation of foliage clumping index using hemispherical photography. *Agric. For. Meteorol.* 149, 1781–1787.
- Goudriaan, J., 1988. The bare bones of leaf-angle distribution in radiation models for canopy photosynthesis and energy exchange. *Agric. For. Meteorol.* 43, 155–169.
- Gower, S.T., Kucharik, C.J., Norman, J.M., 1999. Direct and indirect estimation of leaf area index, fAPAR, and net primary production of terrestrial ecosystems. *Remote Sens. Environ.* 70, 29–51.
- Hu, R., Yan, G., Mu, X., Luo, J., 2014. Indirect measurement of leaf area index on the basis of path length distribution. *Remote Sens. Environ.* 155, 239–247.
- Hu, R., Bournez, E., Cheng, S., Jiang, H., Nerry, F., Landes, T., Saudreau, M., Kastendeuch, P., Najjar, G., Colin, J., 2018a. Estimating the leaf area of an individual tree in urban areas using terrestrial laser scanner and path length distribution model. *ISPRS J. Photogramm. Remote Sens.* 144, 357–368.
- Hu, R., Yan, G., Nerry, F., Liu, Y., Jiang, Y., Wang, S., Chen, Y., Mu, X., Zhang, W., Xie, D., 2018b. Using airborne laser scanner and path length distribution model to quantify clumping effect and estimate leaf area index. *IEEE Trans. Geosci. Remote Sens.* 56, 3196–3209.
- Jiang, H., Cheng, S., Yan, G., Kuusk, A., Hu, R., Tong, Y., Mu, X., Xie, D., Zhang, W., Zhou, G., 2021. Clumping effects in leaf area index retrieval from large-footprint full-waveform LiDAR. In: *IEEE Trans. Geosci. Remote Sens.*
- Jonckheere, I., Fleck, S., Nackaerts, K., Muys, B., Coppin, P., Weiss, M., Baret, F., 2004. Review of methods for in situ leaf area index determination: part I. Theories, sensors and hemispherical photography. *Agric. For. Meteorol.* 121, 19–35.
- Jonckheere, I., Nackaerts, K., Muys, B., van Aardt, J., Coppin, P., 2006. A fractal dimension-based modelling approach for studying the effect of leaf distribution on LAI retrieval in forest canopies. *Ecol. Model.* 197, 179–195.
- Jupp, D.L., Culvenor, D., Lovell, J., Newnham, G., Strahler, A., Woodcock, C., 2009. Estimating forest LAI profiles and structural parameters using a ground-based laser called 'Echidna®'. *Tree Physiol.* 29, 171–181.
- Kötz, B., Schaeppman, M., Morsdorf, F., Bowyer, P., Itten, K., Allgöwer, B., 2004. Radiative transfer modeling within a heterogeneous canopy for estimation of forest fire fuel properties. *Remote Sens. Environ.* 92, 332–344.
- Kuusk, A., Nilson, T., Paas, M., Lang, M., Kuusk, J., 2008. Validation of the forest radiative transfer model FRT. *Remote Sens. Environ.* 112, 51–58.
- Kuusk, A., Kuusk, J., Lang, M., 2009. A dataset for the validation of reflectance models. *Remote Sens. Environ.* 113, 889–892.
- Kuusk, A., Nilson, T., Kuusk, J., Lang, M., 2010. Reflectance spectra of RAMI forest stands in Estonia: simulations and measurements. *Remote Sens. Environ.* 114, 2962–2969.
- Kuusk, A., Lang, M., Kuusk, J., 2013. Database of optical and structural data for the validation of forest radiative transfer models. *Light Scatter. Rev.* 7, 109–148. Springer.
- Lang, A., Xiang, Y., 1986. Estimation of leaf area index from transmission of direct sunlight in discontinuous canopies. *Agric. For. Meteorol.* 37, 229–243.
- Leblanc, S.G., 2002. Correction to the plant canopy gap-size analysis theory used by the tracing radiation and architecture of canopies instrument. *Appl. Opt.* 41, 7667–7670.
- Leblanc, S.G., Chen, J.M., 2001. A practical scheme for correcting multiple scattering effects on optical LAI measurements. *Agric. For. Meteorol.* 110, 125–139.

- Leblanc, S.G., Chen, J.M., Fernandes, R., Deering, D.W., Conley, A., 2005. Methodology comparison for canopy structure parameters extraction from digital hemispherical photography in boreal forests. *Agric. For. Meteorol.* 129, 187–207.
- Li, W., Mu, X., 2021. Using fractal dimension to correct clumping effect in leaf area index measurement by digital cover photography. *Agric. For. Meteorol.* 311, 108695.
- Li, J., Du, Q., Sun, C., 2009. An improved box-counting method for image fractal dimension estimation. *Pattern Recogn.* 42, 2460–2469.
- Miller, E., Norman, J., 1971. A sunfleck theory for plant canopies I. Lengths of sunlit segments along a transect 1. *Agron. J.* 63, 735–738.
- Morsdorf, F., Meier, E., Kötz, B., Itten, K.I., Dobbertin, M., Allgöwer, B., 2004. LIDAR-based geometric reconstruction of boreal type forest stands at single tree level for forest and wildland fire management. *Remote Sens. Environ.* 92, 353–362.
- Morsdorf, F., Kötz, B., Meier, E., Itten, K., Allgöwer, B., 2006. Estimation of LAI and fractional cover from small footprint airborne laser scanning data based on gap fraction. *Remote Sens. Environ.* 104, 50–61.
- Nackaerts, K., Sterckx, S., Coppin, P., 1999. Fractal dimension as correction factor for stand-level indirect leaf area index measurements. In: *Remote Sensing for Earth Science, Ocean, and Sea Ice Applications*. International Society for Optics and Photonics, pp. 80–89.
- Neumann, H., Den Hartog, G., Shaw, R., 1989. Leaf area measurements based on hemispheric photographs and leaf-litter collection in a deciduous forest during autumn leaf-fall. *Agric. For. Meteorol.* 45, 325–345.
- Nilson, T., 1971. A theoretical analysis of the frequency of gaps in plant stands. *Agric. Meteorol.* 8, 25–38.
- Pisek, J., Lang, M., Nilson, T., Korhonen, L., Karu, H., 2011a. Comparison of methods for measuring gap size distribution and canopy nonrandomness at Järvelja RAMI (Radiation transfer model Intercomparison) test sites. *Agric. For. Meteorol.* 151, 365–377.
- Pisek, J., Ryu, Y., Alikas, K., 2011b. Estimating leaf inclination and G-function from leveled digital camera photography in broadleaf canopies. *Trees* 25, 919–924.
- Qi, J., Xie, D., Yin, T., Yan, G., Gastellu-Etchegorry, J.-P., Li, L., Zhang, W., Mu, X., Norford, L.K., 2019. LESS: Large-scale remote sensing data and image simulation framework over heterogeneous 3D scenes. *Remote Sens. Environ.* 221, 695–706.
- Qu, Y., Zhu, Y., Han, W., Wang, J., Ma, M., 2013. Crop leaf area index observations with a wireless sensor network and its potential for validating remote sensing products. *IEEE J. Sel. Top. Appl. Earth Obs. Remote Sens.* 7, 431–444.
- Ross, J., 1981. *The Radiation Regime and Architecture of Plant Stands*. Springer Science & Business Media.
- Ryu, Y., Nilson, T., Kobayashi, H., Sonnentag, O., Law, B.E., Baldocchi, D.D., 2010. On the correct estimation of effective leaf area index: does it reveal information on clumping effects? *Agric. For. Meteorol.* 150, 463–472.
- Song, W., Mu, X., Yan, G., Huang, S., 2015. Extracting the green fractional vegetation cover from digital images using a shadow-resistant algorithm (SHAR-LABFVC). *Remote Sens.* 7, 10425–10443.
- Stark, S.C., Leitold, V., Wu, J.L., Hunter, M.O., de Castilho, C.V., Costa, F.R., McMahon, S.M., Parker, G.G., Shimabukuro, M.T., Lefsky, M.A., 2012. Amazon forest carbon dynamics predicted by profiles of canopy leaf area and light environment. *Ecol. Lett.* 15, 1406–1414.
- Stenberg, P., 1996. Correcting LAI-2000 estimates for the clumping of needles in shoots of conifers. *Agric. For. Meteorol.* 79, 1–8.
- Stenberg, P., Möttus, M., Rautiainen, M., Sievänen, R., 2014. Quantitative characterization of clumping in scots pine crowns. *Ann. Bot.* 114, 689–694.
- Walter, J.-M.N., Fournier, R.A., Soudani, K., Meyer, E., 2003. Integrating clumping effects in forest canopy structure: an assessment through hemispherical photographs. *Can. J. Remote. Sens.* 29, 388–410.
- Wang, W.-M., Li, Z.-L., Su, H.-B., 2007. Comparison of leaf angle distribution functions: effects on extinction coefficient and fraction of sunlit foliage. *Agric. For. Meteorol.* 143, 106–122.
- Wilson, J.W., 1960. Inclined point quadrats. *New Phytol.* 59, 1–7.
- Wilson, J.W., 1963. Estimation of foliage denseness and foliage angle by inclined point quadrats. *Aust. J. Bot.* 11, 95–105.
- Yan, G., Hu, R., Wang, Y., Ren, H., Song, W., Qi, J., Chen, L., 2016. Scale effect in indirect measurement of leaf area index. *IEEE Trans. Geosci. Remote Sens.* 54, 3475–3484.
- Yan, G., Hu, R., Luo, J., Weiss, M., Jiang, H., Mu, X., Xie, D., Zhang, W., 2019. Review of indirect optical measurements of leaf area index: recent advances, challenges, and perspectives. *Agric. For. Meteorol.* 265, 390–411.
- Yan, G., Jiang, H., Luo, J., Mu, X., Li, F., Qi, J., Hu, R., Xie, D., Zhou, G., 2021. Quantitative evaluation of leaf inclination angle distribution on leaf area index retrieval of coniferous canopies. *J. Remote Sens.* 2021.
- Zou, J., Yan, G., Zhu, L., Zhang, W., 2009. Woody-to-total area ratio determination with a multispectral canopy imager. *Tree Physiol.* 29, 1069–1080.
- Zou, J., Leng, P., Hou, W., Zhong, P., Chen, L., Mai, C., Qian, Y., Zuo, Y., 2018. Evaluating two optical methods of woody-to-total area ratio with destructive measurements at five *Larix gmelinii* rupForest Plots China. *Forests* 9, 746.
- Zou, J., Zuo, Y., Zhong, P., Hou, W., Leng, P., Chen, B., 2020. Performance of four optical methods in estimating leaf area index at elementary sampling unit of *Larix principis-rupprechtii* forests. *Forests* 11, 30.